THESIS

This is to certify that the

thesis entitled

Thermal Conductivity of Solid Argon

presented by

Juan Javier Bautista

has been accepted towards fulfillment
of the requirements for

Ph.D. degree in Physics

Gerald L. Pollack
Major professor

Date April 4, 1980

O-7639

THERMAL CONDUCTIVITY OF SOLID ARGON

By

Juan Javier Bautista

A DISSERTATION

Submitted to

Michigan State University

in partial fulfillment of the requirements

for the degree of

DOCTOR OF PHILOSOPHY

Department of Physics

1980

ABSTRACT

THERMAL CONDUCTIVITY OF SOLID ARGON

By

Juan Javier Bautista

An apparatus was designed and constructed to measure the thermal conductivity of rapidly cooled samples of solid argon grown from the melt. A linear heat flow method was used to obtain the *in situ* measurements while the samples were under their own equilibrium vapor pressure in the temperature range of 2.2 K to 83 K. The measurements obtained indicated the presence of a thermal contact resistance which was quantitatively taken into account.

The corrected data are in reasonable agreement with the constant and equilibrium volume data of previous experimenters. In addition, the present data are of sufficient density to compare to previous theoretical calculations.

To Simona, Carlye and Geraldo

ACKNOWLEDGMENTS

I would like to express my extreme gratitude and appreciation to Professor G. L. Pollack for his unyielding support and encouragement throughout the course of this research and my graduate career at Michigan State University. I would also like to thank Professors J. Kovacs, S. D. Mahanti and T. Kaplan for their support and especially Professor J. Cowen who provided suggestions and guidance at crucial moments.

I am also greatly indebted to my wife, Simona, for her patience, love and support throughout our stay at Michigan State University. I would also like to thank her for her dedication and persistence toward the typing and completion of this manuscript. I would also like to thank Rob Godbey for his assistance in preparing some of the figures.

Finally, I would like to thank the Michigan State University Physics Department, the Department of Energy (formerly E. R. D. A.) and the Ford Foundation for contributing to the financial support of this work.

TABLE OF CONTENTS

LIST OF APPENDICES

LIST OF TABLES

LIST OF FIGURES

I. INTRODUCTION

A. Discovery and General Properties of the Rare-Gas Solids

Historically, the first of the rare-gases to be identified was argon (Ar). In 1785 Henry Cavendish was the first to observe argon while attempting to identify the constituents of atmospheric air.[1] However, it wasn't until approximately a century later that the "lazy one", argon, was identified as a new element by Lord Rayleigh and Sir William Ramsay. Subsequently, Ramsay within a short span of four years went on to discover the rest of the elements (He, Ne, Xe and Kr) comprising the eighth column of the periodic table with the exception of radon (Rn) which was discovered two years later by Ernest Rutherford.[2]

Since the introduction of quantum physics the scientific community has devoted considerable attention to the problem of understanding the properties of the rare-gas solids. Although the bulk of the work has been devoted to lattice dynamics,[3] work has also been carried out over a wider range. For example, there have been recent studies of the interaction of gaseous xenon with biological materials,[4,5] and also recently, solid xenon has been converted from an insulator to a conductor by the application of very high

pressures.[6] Of the solid state properties of rare-gas solids (RGS) investigated to date the relatively least understood is thermal conductivity.[7]

Although the rare-gas solids are easily exploited as theoretical models, they are less amenable to experimental handling. The rare-gas solids are well suited for theoretical thermal conductivity studies since they form simple close packed structures containing one atom per unit cell and are, ordinarily, electrical insulators due to their closed shell electronic structure.[8] Hence, when thermal conductivity is to be investigated it is only necessary to consider the heat transported by lattice vibrational waves. The complicating effects due to the heat transport of conduction electrons present in metals and semiconductors or due to optic modes occurring in solids with more than one atom per unit cell can safely be ignored. Furthermore, the intermolecular forces are essentially central in nature and the lattice dynamics are relatively well understood.[7]

B. Thermal Conductivity of an Insulator

The specific question that currently arises is the following: What can one learn by investigating the thermal conductivity of an insulator? The answer is that since heat is transported by atomic vibrations in insulators one can gain valuable information about their nature. The thermal conductivity for these materials is entirely determined by the way in which lattice vibrational waves (phonons) interact with one another and how they interact with defects,

impurities and the sample boundaries.[9]

For the purposes of calculation the total lattice potential may be expanded in a Taylor series in terms of the displacements of the atoms from their equilibrium sites. For small oscillations the harmonic term is taken to represent the ideal crystal, while the higher order terms are then treated as perturbations.[10] The energy of these lattice vibrations or phonons is quantized with one phonon having energy $E = \hbar\omega$ and crystal momentum $\vec{p} = \hbar\vec{q}$ (where ω is the phonon frequency and $\vec{q}$ is the phonon wave vector). The average number of phonons having this energy is given by the Planck distribution

$$n(\omega) = 1/(\exp(\hbar\omega/k_B T)-1) \qquad (1)$$

where k_B = Boltzmann constant.

Hence one can view a finite insulating solid as a rigid-walled box containing a phonon gas. By heating one end of the box we locally increase the number of phonons having energy $\hbar\omega$. These will then tend to diffuse toward the cooler end and a net flow of energy will result. A useful expression for the thermal conductivity of an insulator is given by

$$\kappa = (1/3)C_v \upsilon \ell \qquad (2)$$

where C_v is the specific heat per unit volume at constant volume, υ the velocity of sound and ℓ the phonon mean free path.[11] It should be pointed out that although Equation (2) also gives the thermal conductivity for an ideal classical gas, the number of phonons (or particles) does not remain constant as in the case for a classical gas.

Although Equation (2) is not accurate in general, it can be used to gain valid physical insights. Since the specific heat C_v is a well known function of temperature and the velocity of sound υ is not strongly temperature dependent, it is then only necessary to define the mean free path ℓ. In general ℓ is a very complicated function of temperature and frequency. However, in order to gain a good qualitative understanding it is sufficient to consider the mean free path characteristic of the dominant scattering mechanism.

For temperatures above the Debye temperature (Θ), C_v is constant and the mean free path is proportional to the inverse of the temperature (T^{-1}). Thus κ is proportional to T^{-1}. Since phonons cannot interact (scatter from one another) in the harmonic approximation this behavior is entirely explained by the anharmonic terms in the Taylor series which couples the phonons. That is, a phonon may now combine with a second to give a third or it may break up to give two phonons.

Although it may be obvious that $\ell \propto T^{-1}$ (since $\ell \propto 1/n$ and $n \to k_B T/\hbar\omega$ as $T \to \infty$), not all of the phonon-phonon interactions contribute to the thermal resistivity. Only the so called Umklapp processes contribute directly to the thermal resistivity ($1/\kappa$) while the normal processes only redistribute the phonon energies. Although normal processes do not contribute directly to the thermal resistivity, they do contribute indirectly by keeping those states occupied which scatter by Umklapp processes.

This can be understood by considering the conservation rules for combining two phonons to produce a third inside a crystal. These are the energy conservation

$$\hbar\omega_1 + \hbar\omega_2 = \hbar\omega_3 \tag{3}$$

and wave vector conservation given by

$$\vec{q}_1 + \vec{q}_2 = \vec{q}_3 \pm \vec{K} \ . \tag{4}$$

Here $\vec{K}$ is a reciprocal lattice vector of the crystal. When $\vec{K} = 0$ in Equation (4) the scattering processes are called normal processes and when $\vec{K} \neq 0$ Umklapp processes.[12]

To simplify the argument we will consider the interaction of two phonons in a one dimensional solid of lattice spacing a. Figure 1(a) illustrates two phonons combining to yield a third that is within the first Brillouin zone. Normal processes do not change the direction of energy flow, hence cannot directly contribute to the thermal resistivity. In Figure 1(b) the phonons combine to yield a third that lies outside the first Brillouin zone. This phonon is equivalent to one lying within the first zone but pointing in the opposite direction. For this case there has been a reversal of energy flow, hence only Umklapp processes contribute directly to the thermal resistance.

As the temperature is lowered toward the Debye temperature the number of phonons present that can participate in Umklapp scattering decreases exponentially, i.e. $n \propto \exp-(\Theta/bT)$. Thus the thermal conductivity will increase exponentially as the temperature is lowered further.[7]

For a perfect infinite solid the mean free path would

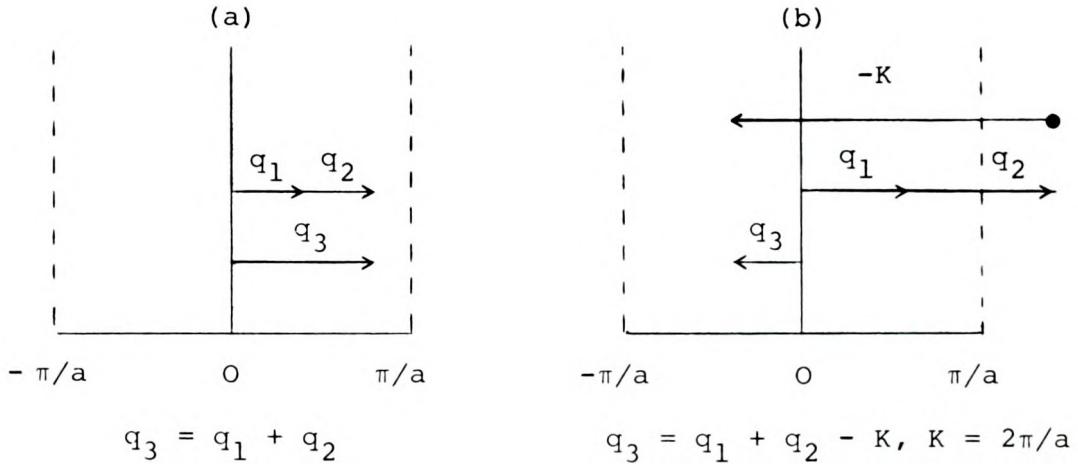

Figure 1. (a) A normal process and (b) an Umklapp process in a one dimensional crystal of lattice constant a.

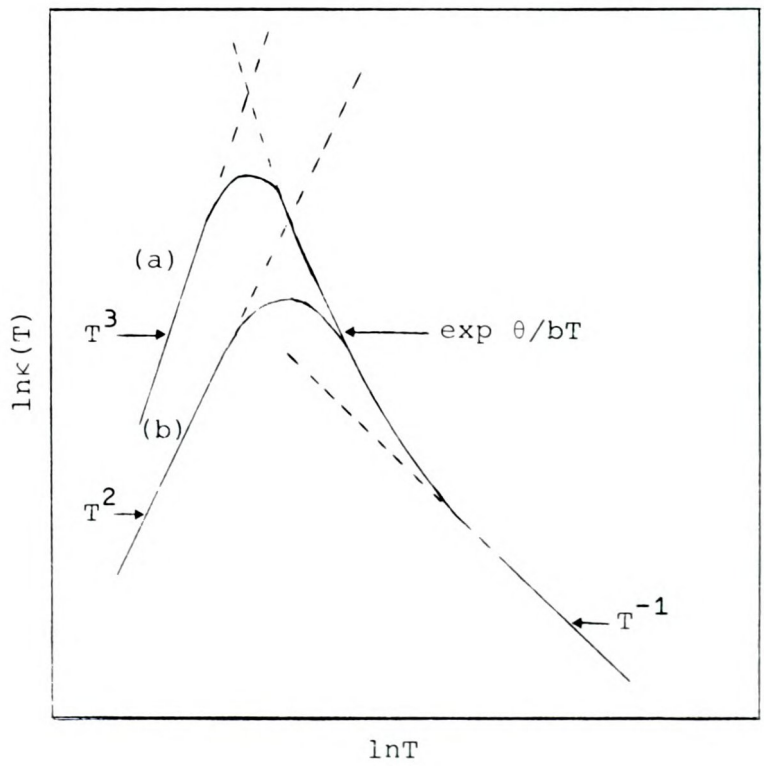

Figure 2. Typical behavior of thermal conductivity for (a) a finite crystal with no defects and (b) a crystal with dislocations.

continue to rise exponentially without bound as the temperature is lowered significantly past the Debye temperature. However for a finite but otherwise perfect solid the mean free path will become constant and of the order of the dimensions of the solid. That is, phonons propagate without scattering to the surface of the solid where they are absorbed and reemitted. Thus at very low temperatures the thermal conductivity will be proportional to the specific heat, i.e. $\kappa \propto T^3$ for a perfect but finite solid.

For defected solids the mean free path is determined by the type of defects and their concentration. The kinds of defects that concern us are point defects (vacancies, impurities, isotopic impurities and interstitials) and line defects (dislocations).

At low temperatures the mean free path due to phonon scattering from imperfections is not intrinsically temperature dependent. It is strongly dependent on the phonon frequency ω. Hence in order to establish the temperature dependence of the thermal conductivity associated with a particular type of defect a slightly more complex expression than Equation (2) is needed.

It can be shown that in the Debye approximation ($\omega = \upsilon q$) for a cubic and isotropic crystal the thermal conductivity is given by

$$\kappa(T) = k_B \upsilon / 2\pi^2 (k_B/\hbar\upsilon)^3 T^3 \int_0^{\Theta/T} x^4 \exp x (\exp x - 1)^{-2} \ell(q(x)) dx \quad (5)$$

where Θ = Debye temperature and $x = \hbar\omega/k_B T$, a dimensionless

variable. In the special case where only one type of defect is present in the crystal $\ell(q(x))$ can be adequately represented by a power law of the form

$$\ell(q(x)) = Aq^{-n} = A(\kappa_B T/\hbar\upsilon)^{-n} x^{-n} \quad . \tag{6}$$

If we now take the low temperature limit ($T<<\Theta$) we note that equation (5) yields that

$$\kappa(T) = B_n T^{3-n} \tag{7}$$

where $B_n = k_B\upsilon/2\pi^2(k_B/\hbar\upsilon)^{3-n} A\int_0^\infty x^4 \exp x(\exp x-1)^{-2} dx$.[13]

Although quantum mechanical perturbations methods are required to obtain the exact expressions for $\ell(q)$, we will for the present rely on useful classical analogs that are reasonable approximations for phonons of long wavelengths. As we shall see this is a valid assumption at low temperatures.

Defects in a solid tend to distort (or strain) the lattice within their vicinity. This defective region will in general have slightly different physical characteristics (e.g. density, compressibility, etc.) than the surrounding region and hence scatter incoming phonons.[14]

A phonon scattering from a point defect is analogous to the scattering of a plane sound wave from a fixed solid sphere. Rayleigh showed that in the long wavelength the limit, i.e. $\lambda>>V^{1/3}$ where V = volume of the sphere, the intensity of the scattered sound wave is proportional to q^4 (see Appendix C).[15] Phonons of wavelengths greater than the dimensions of the defect (a few lattice spacings) will

then display a mean free path that is inversely proportional to q^4 (since $\ell(q) \propto 1/\sigma(q)$). Thus at low temperatures a solid with only point defects present will have $\kappa \propto T^{-1}$.

The scattering of phonons from static dislocations is characterized by two main features. These are the core of the dislocation consisting of a narrow region along its axis and the surrounding strain field (whose radial extension is of the order of several wavelengths). The strain of the crystal about the dislocation varies as b/r where b = Burgers vector of the dislocation and r = radial distance from the core.

To incident phonons the core can be regarded as a long and narrow cylindrical obstruction with cross sectional area $A = \pi a^2$. Rayleigh also showed that in the long wavelength limit ($\lambda >> A^{1/2}$) the scattering cross-section per unit length of dislocation varies as $a(a/\lambda)^3$ (see Appendix C).[15] Thus ℓ_{core} is proportional to q^{-3}.

For the surrounding strain field the Rayleigh theory is not applicable, since $\lambda \gtrsim A^{1/2}$. The effect of the surrounding strain field can be estimated by considering an analogy with geometrical optics. As a phonon passes through the strained region the phonon's velocity will be altered due to the anharmonicity in real crystals. The phonon velocity in this region is given by

$$\upsilon = \upsilon_0(1 \pm \gamma b/r) \qquad (8)$$

where υ_0 = velocity in the unstrained region, and γ is the Grueneisen constant (a measure of the anharmonicity). To

first order for small scattering angles the incident phonon will be deviated from its original direction by an angle $\phi \sim \gamma b/p$ where p is approximately the closest distance that the phonon will approach the dislocation core. For a small scattering angle ϕ the scattering cross-section per unit length of dislocation will be proportional to $\gamma^2 b^2/p_0$ where p_0 is the smallest allowed value for p. Our geometrical optics analogy breaks down unless $p_0 \gtrsim \lambda$. Hence, the scattering cross-section is proportional to q and thus $\ell_{strain} \propto q^{-1}$.[16,17]

The ratio of the mean free paths is thus $\ell_{strain}/\ell_{core}$ which varies as $a(a/\lambda)^3/(\gamma^2 b^2/\lambda)$. Since $\gamma \simeq 1$, $\ell_{strain}/\ell_{core}$ thus varies as $(a^4/\gamma^2 b^2)/\lambda^2 \simeq (a^2/b)^2/\lambda^2$. In the low temperature region the wavelength of a typical phonon is much greater than both the dislocation core radius a and the Burgers vector b, hence $\ell_{strain} << \ell_{core}$. Thus a defective solid dominated by dislocations will display a thermal conductivity that is proportional to T^2.[14]

Therefore $\kappa(T)$ is seen to be a sensitive indicator of crystalline quality at low temperatures, while at the higher temperatures it is a sensitive indicator of the interatomic potential anharmonicity. Figure 2 contains a graph of the thermal conductivity of an insulator displaying the main features we have just discussed.

C. Thermal Conductivity of Solid Argon- Experimental Background

Since the intermolecular forces are weak and short ranged the RGS are characterized by low melting temperatures, high vapor and sublimation pressures and a relatively large ratio of heat of fusion to heat of vaporization, it is necessary to carry out experiments at cryogenic temperatures and/or high pressures.[8,54] In addition, since the probability of stray nucleation is relatively high, large grained single crystals are difficult to obtain. The difficulty of obtaining a defect free sample is compounded by the small activation energies necessary for inducing various types of crystal defects and an unusually large thermal expansivity which may well be 100 times larger than that of the container it is grown in. Hence, experimenters must be content to work with plastic and easily deformed solids at low temperatures.[8,18]

The thermal conductivity for an isotropic solid is defined by the relation

$$\vec{h} = -\kappa \vec{\nabla} T \tag{9}$$

where $\vec{h}$ is the heat flux, $\vec{\nabla} T$ is the temperature gradient and the constant of proportionality κ is the thermal conductivity. Hence in order to measure the thermal conductivity in principle it is only necessary to know the heat flux and the temperature gradient associated with it.

To date six groups have measured the thermal conductivity of solid Ar.[7,19,20,21,22,23,24,25] These experiments

can be classified as either constant volume or equilibrium volume measurements. There are of course inherent trade-offs when one choses to perform one type of experiment over another.

The major disadvantage of performing constant volume measurements is that high pressures must be applied. Hence chambers containing the samples are necessarily opaque and usually have thermal conductivities comparable to the sample itself. This latter problem may be partially obviated in one of two ways depending upon the geometry employed for the measurements.

First, the standard, direct linear heat flow method may be employed for constant volume measurements. In this method heat is conducted parallel to the sample walls. Now the thermal conductivity of solid Ar at high temperatures is comparable to that of glass. This is usually much smaller than the thermal conductivity of a typical metal sample chamber. Thus, this method has the disadvantage of tending to make the high temperature region very difficult to measure.

A second method that may be chosen is the radial heat flow method. In this method heat is conducted radially outward toward and perpendicular to the sample chamber walls. Since the sample chamber can be chosen to have a large heat capacity and thermal conductivity, it can be used as a heat sink that defines a thermal equipotential surface.[23] This method has the advantage over the first

that most of the heat is carried by the sample itself, hence measurements can be carried out over the entire temperature range without difficulty.[7]

Once the difficulties associated with the application of high pressures to RGS are overcome, the thermal conductivity as a function of T at constant volume can be studied as well as the thermal conductivity as a function of density at constant T.[7] Furthermore, since the volume is kept constant, the sample is usually in good thermal contact with the heat sinks and the temperature probes throughout.

The major drawback associated with equilibrium volume experiments is the unusually large thermal expansivity of solid Ar. In cooling down from its triple point (83.8 K) to liquid helium temperatures the volume of the sample of Ar will contract approximately 9%, hence the temperature probes as well as the thermal heat sinks will tend to pull away from the sample. The thermal contact problem is also aggravated by the vapor phase transport of material from the heat sinks and probes in the presence of a thermal gradient. This causes the formation of voids about the heat sinks and probes.[8] Furthermore, a small yield strength near the triple point and relatively high brittleness at low temperatures make the introduction of defects particularly easy whenever large thermal gradients are introduced.[26]

Hence in spite of the difficulties mentioned so far, the major advantage of the equilibrium volume method is that the application of high pressures are not required so

that transparent, thin-walled and low thermal conductivity sample tubes can be employed. The advantages of using this type of sample tube are that most of the heat will be conducted by the sample throughout the entire temperature range of interest; and one can visually inspect the quality of the sample at any time during an experiment. Another advantage is that it has been demonstrated that growing Ar crystals from the melt at equilibrium volume is the best method so far for growing single crystals.[27]

To date all of the thermal conductivity experiments performed at equilibrium volume have employed a linear steady-state heat flow method. Of the samples examined most were grown from the melt using a Bridgman technique. That is, the samples were directionally grown solidifying from bottom to top as heat was extracted from the bottom of the sample tube. Although the sizes of the samples varied all were cylindrical. As was mentioned earlier, since these samples are allowed to contract the thermal boundary resistance at the heat sinks, probes, and other interfaces may not have been properly taken into account.

White and Woods[19] were the first to measure the thermal conductivity of solid neon, argon and xenon. Their samples were grown from the melt in thin-walled Inconel tubes of 1.3 cm diameter by 7.6 cm length. The temperature difference was measured by two He gas thermometers connected to two copper wires approximately 5 cm apart.[28] These wires were in turn stuck through the tube perpendicular to the axis

of the sample tube and soldered in place.

Although White and Woods were not able to visually examine their samples, they were able to estimate the quality of their samples from trial experiments performed using a glass sample tube. From these they estimated that the growth rates varied from 1 to 2 mm/min. For these growth rates one might expect grain sizes between 0.1 and 1 mm.[26] The trial samples were initially transparent and were found to become opaque and cloudy when rapidly cooled from 77 K to 4 K.

The results of their thermal conductivity measurements supported their preliminary observations. The six samples they studied displayed very low thermal conductivity values at low temperatures, indicating that they were highly defective due to the constraints imposed by the sample tube during cooling. It was further noted that the fifth sample yielded the lowest values even though greater care was exercised to minimize the thermal strains.[19] This result may have been caused by the loss of good thermal contact. Since this sample was cooled at a slower rate than previous samples a significant amount of mass migration through the vapor phase may have occurred at the thermal probes.

Bernè, Boato and DePaz[22] cognizant of the difficulties encountered by White and Woods[19] succeeded in eliminating some of the earlier experimental difficulties. Bernè et al. grew over 50 samples of solid argon from the melt. Only 12 of these yielded data. These specimens were grown in pyrex

tubes (0.55 cm inner diameter by 6 cm long) at rates of 1 to 3 mm/hr (1/60 of the rates used by White and Woods). The average grain sizes were observed to be between 1 and 4 mm. In addition, the thermal strains induced by the container were completely removed.

After the sample was grown, near the triple point temperature, it was cooled down to a uniform temperature of about 75 K. The sample was then separated from the container walls by subliming a small amount of material at the sample chamber walls. This was accomplished by pumping gently on the vapor above the sample.[27] Once the sample was completely separated, it was lifted out of its container by means of a pyrex rod which was embedded in the top of the sample during crystal growth. The sample was then positioned between four copper spring clamps that were anchored to the conductivity measuring stage of the apparatus (a heat source, two helium gas thermometers and a heat sink).

To prevent the sample from subliming further and to reduce the thermal gradients during cooldown the sample was surrounded by helium exchange gas at a pressure of 200 Torr. The samples were then slowly cooled to 4 K. Although the sample was slightly reduced in size (since some sublimation nonetheless occured), the samples remained optically transparent.

With the sample at 4 K the clamps were then closed, gripping the sample, and the measurements were performed.

Spring clamps of moderate strength were used, since it was found that clamps which were too strong would break the sample and clamps which were too weak would achieve very poor thermal contact.

Since the vapor pressure of argon increases quite rapidly as the temperature is increased Bernè, et al. confined their measurements to low temperatures between 3 K and 15 K. Although their values were much higher than those obtained by White and Woods (indicating better quality samples), the data were not reproducible from sample to sample as well as for a single sample. This was attributed to the different ways in which the samples were grown and to thermal contact which may have varied from sample to sample.

Krupskii and Manzhelii[20] unlike Bernè, et al. concentrated their efforts on making precise measurements at high temperatures. Three specimens were grown from the vapor at 70 K in glass sample tubes (1.9 cm inner diameter by 5 cm length) at rates less than 5 mm/hr and the expected grain sizes are of 1 to 4 mm.[27] To measure the thermal gradient the sample was conveniently grown about a differential copper-constantan thermocouple.

Since their work covered the temperature range of 24 K to 73 K, where the thermal conductivity is defect independent, Krupskii and Manzhelii made no attempt to remove the strains induced by the sample chamber.[20] By cooling their samples slowly at rates of 10 K/hr to the desired temperature,

Krupskii and Manzhelii were able to keep all but one of the samples free of any visible defects. That is, the first two samples remained transparent while the third became translucent after cooling. The data of Krupskii and Manzhelii were nonetheless reproducible from sample to sample.

As with other workers, Krupskii and Manzhelii also experienced trouble with loss of thermal contact at the heat sink and source as the sample was cooled. This problem was partially overcome by the introduction of He gas into the sample chamber to reestablish contact.

Since it was established by Peterson, et al.[27] that crystals grown from the vapor are much more defective than those grown from the melt, it is mildly surprising that at about 25 K Krupskii and Manzhelii obtained higher values of thermal conductivity than White and Woods. Krupskii and Manzhelii attributed this difference to having obtained better quality crystals than White and Woods. However, a more likely explanation is that Krupskii and Manzhelii obtained better thermal contact than White and Woods, since at 25 K the thermal conductivity is essentially defect independent.

Christen and Pollack[24] unlike previous workers attempted to remove both the thermal boundary resistance (at the temperature probes, heat source and heat sink) and the thermal strains. The samples tested were grown from a "seed" in a thin, transparent Mylar tube (1 cm diameter by 3 cm length) at the rate of 0.7 mm/hr. The seed was prepared by locally

maintaining the bottom the liquid filled sample tube slightly below the Ar triple point temperature until a thin wafer of solid about 0.5 mm thick appeared. It was then allowed to anneal for a period of 12 to 24 hours before the remainder of the sample was grown. It was observed that samples prepared in this way had grains which were 5 mm to 10 mm in size.[25]

The principal difference between the measurements performed by Christen and Pollack and those of other workers was the number and the location of the thermometers used to measure the temperature gradient. Since argon tends upon cooling to separate from the temperature probes, a single germanium thermometer was embedded in the heat source located at the bottom of the sample tube. The temperature difference between the top and the bottom was measured in the following way. First, the entire sample was allowed to reach a uniform temperature. In this case the temperature was that of the heat sink situated at the top of the sample. This was accomplished by electronically controlling the heat needed to keep the heat sink at a constant temperature. This initial temperature was noted and then heat was applied to the bottom of the sample via the heat source located there. Once a steady-state condition was reached, the temperature at the heat source was once again noted. Hence, assuming a thermal contact resistance was not present at the interfaces the temperature gradient along the sample is the difference between the final and initial temperatures at the

heat source divided by the length of the sample.

To reduce thermal strains Christen and Pollack first partly detached the sample from the walls of the sample chamber in essentially the same manner employed by Berne`, et al. Once separated the samples were cooled to liquid helium temperatures at the rate of 1 K/hr.

To prevent the sample from separating from the heat source and sink the sample tube was lifted toward the heat sink during cooling. This was accomplished by the use of a metal bellows attached to the top of the sample tube. Due to the high vapor pressure of argon near 83.8 K an over-pressure of over half an atmosphere keeps the bellows expanded. As the temperature is lowered the vapor pressure drops quite rapidly[8] and hence nearly a constant positive stress is exerted on the sample as the temperature is lowered further.

In order to prevent atoms from migrating away from the interface between the heat source and the bottom of the sample during the cooling process Christen and Pollack kept the bottom of the sample slightly colder than the top. This was accomplished by the introduction of a small amount of helium exchange gas around the sample tube. It should be noted that the presence of this thermal gradient tends to encourage migration of atoms toward the bottom of the sample. Thus possibly reducing the contact area at the interface between the heat sink and the top of the sample.

Of the 10 samples grown by Christen and Pollack only

three yielded low temperature data. The data were found to be reproducible for a given sample but not from sample to sample. Most of the samples were found to turn cloudy and all suffered at least some surface defects on cooling. This was attributed to the sample bridging to and subsequently separating from the walls of the sample chamber.

To check for a thermal boundary resistance Christen and Pollack measured two samples of different lengths. If the thermal contact resistance ($1/K_{Cont}$) and the thermal resistivity ($1/\kappa$) is the same for both samples, then the effective thermal resistance ($1/K_{Eff}$) should be a linear function of the lengths with a positive non zero y-intercept ($1/K_{Cont}$). Quantitatively expressed we have

$$1/K_{Eff} = L/\kappa A + 1/K_{Cont} \qquad (10)$$

where

$$K_{Eff} = \dot{Q}/\Delta T \quad . \qquad (11)$$

In Equations (10) and (11) K_{Eff} is the effective (or measured) thermal conductance, L is the length of the sample and A is its cross sectional area, κ is the thermal conductivity of the argon crystal, K_{Cont} is the thermal contact conductance, $\dot{Q}$ is the power supplied to the heat source and ΔT is the temperature difference between the heat source and sink associated with the application of $\dot{Q}$. Since their two samples yielded results that implied that $1/K_{Cont}$ was a negative quantity Christen and Pollack assumed that a thermal boundary resistance was either not present or negligible.[25]

In view of the great care exercised in handling the samples it is surprising the data at low temperatures indicated that these samples were only slightly better than those tested by White and Woods.[19] It should be pointed out that in Equation (10) κ and K_{Cont} could have also changed for the two samples tested by Christen and Pollack. Ideally, the same sample of two different lengths would have been preferred. The possibility of the existence of a boundary effect should not have been so easily dismissed, since it may have been, in fact probably was, present.

Clayton and Batchelder[23] were the first workers to perform constant volume thermal conductivity measurements. Their work has been recognized as the first direct verification of one of the oldest predictions of solid state physics. In 1914 Debye[9] showed that at high temperatures the thermal conductivity at constant volume should be inversely proportional to the temperature. Clayton and Batchelder's experiments showed that this prediction is valid.

For this extremely difficult experiment,[23] 5 samples of various molar volumes were grown from the melt at essentially constant pressure. The pressures used to grow the samples were in the 1 to 5 kilobar range. A high thermally conducting copper tube (7.0 cm long and 1.5 cm i.d.) contained within a high pressure cell served as the sample chamber.

The thermal conductivity measuring part of the apparatus was located within the sample chamber tube concentric

with the tube's axis. The heat source was constructed of a long thin steel rod wound with heater wire which lay along the tube axis. Two concentric copper rings suspended with nylon string served to define two thermal equipotentials. A difference thermocouple attached to the two rings measured an average radial temperature difference.

These samples were grown from the melt at constant pressure in a manner similar to that of Crawford and Daniels,[29] Daniels, et al.[30] and Leake, et al.[31] Before a sample was grown it was first determined what the melting temperature and pressure should be such that at a given temperature the sample experienced no external pressure. The sample chamber is filled with liquid at the temperature T_m and a pressure slightly less than P_m and left to equilibrate for several hours. Next, in the presence of a slight thermal gradient along the length of the sample chamber the pressure was gradually increased to P_m and crystallization was marked by a momentary rise in temperature. As solid continued to fill the sample chamber more argon was introduced to maintain a constant pressure.[26] The samples were then left to anneal for 16 to 39 hours near their respective melting temperatures.

Although the samples could not be visually examined, the low-temperature thermal conductivity data obtained by Clayton and Batchelder[23] indicated that the samples were of the same quality as those grown by Bernè, et al. Although Clayton and Batchelder had no direct way to test for

a thermal contact resistance, it is unlikely that one was present, since the external pressure on the samples is not expected to pass through zero.

The nylon string used to support the concentric copper rings aided Clayton and Batchelder in determining the strained state of their samples. That is, if the strings were found broken after performing an experiment, it was assumed that the samples had been severely strained and the data were discarded.

Clayton and Batchelder found that for a given sample the data were reproducible for the entire temperature range investigated, except in a small region slightly below the melting temperature. Between the melting temperature and just 20 K below it their data fluctuated randomly. The instability in this region was attributed to significant recrystallization of the sample during the measurements.

It has been demonstrated that samples grown at high pressures consist of a large single crystal surrounded by many small ones[26] having grains of 1 to 10 mm in size. This is a consequence of the high thermal conductivity of the sample chamber walls.

One of the experimental difficulties encountered by Clayton and Batchelder was that near the thermal conductivity maximum the error in measuring the temperature difference was largest. Near the maximum they found that the relatively larger amount of power required to produce a measurable temperature difference caused an appreciable

warming of the sample. It was later suggested by Clayton and Batchelder that this difficulty could be overcome by employing a linear heat flow method.

Weston and Daniels[7] subsequently pursued this suggestion and performed measurements at constant volume near the conductivity maximum. The temperature range covered was between 5 K and 40 K. Weston and Daniels' sample preparation techniques were similar to Clayton and Batchelder's. However, the results of their work indicated that their samples were of a significantly better quality, than those studied by previous workers.

D. Purpose

In view of the difficulties experienced by previous experimenters with the thermal contact resistance, one of our chief interests was to determine what role, if any, the thermal contact resistance plays in the measurement of the thermal conductivity of solid Ar at equilibrium pressures. Once this was determined our next goal was to provide reliable data so that the various theoretical models currently available can be tested.

Natural Ar was chosen because of its value as a research material. Its low triple point temperature (83.8 K) allows the use of inexpensive liquid nitrogen as the cryogen during crystal growth. The interatomic potential is the best known of all the rare gases. Natural argon is relatively inexpensive and is available in very pure form (less then 10 ppm total impurity content) and is nearly isotopically

pure. The argon content of atmospheric air is 99.6% Ar^{40}, 0.337% Ar^{36} and 0.063% Ar^{38}.[2]

For the present work we grew several crystalline samples of Ar under controlled conditions. The measurements of the effective thermal conductance were all performed in situ. We first measured the effective thermal conductance at constant temperature as a function of the force applied to the ends of the crystal at the heat source and sink interfaces. We then measured the effective thermal conductance for various sample lengths while we varied the temperature.

The data obtained from these experiments will be compared to those of previous experimental and theoretical workers.

II. THE EXPERIMENT

A. Cryogenic Apparatus

To perform the current experiments an apparatus was designed and constructed to measure thermal conductivity at low temperatures. The apparatus was mounted within a double dewar system to allow the use of liquid He or liquid N_2 as the cryogen.

1. Description of Apparatus

The design of the apparatus is similar in principle to the steady-state linear heat flow systems used by previous workers.[19,20,22,24] In particular, it is patterned on the system employed by Christen and Pollack.[24] Although the present system incorporates many of the same features as theirs, the use and construction of the sample chamber is considerably different. A sketch of the cryostat is shown in Figure 3.

The cylindrical sample chamber was constructed from a sheet of transparent Mylar 0.005" in thickness. A tube 3 to 4 cm long was formed by gently heating the Mylar sheet with a heat gun while it was wrapped tightly around a Teflon mandrel until it conformed to the mandrel. The seam was then secured with ordinary quick-setting epoxy glue.

A - Ar Gas Line
B - He Gas Line
C - Brass Gears
D - Upper Cu (Block) Heat Sink
E - Pt Sensor
E'- Ge Sensor
F - Ar Needle Valve
G - Threaded Brass Rods
H - Large Cu Bellows
I - Vacuum Chamber
J - Short Cu Bellows
K - Sample Tube Cu Flange
L - Mylar Sample Chamber
M - Al Lower Block Heater
N - Ge Thermometer
N'- Pt Thermometer
O - Stainless Steel Tube
P - He Needle Value
Q - Braided Cu Wire
R - Upper Block Heater
S - Exchange Gas Chamber
T - Cu Lifting Flange
U - Cu Piston
V - Cotton Thread
W - Annular Heater
X - Cu Radiation Shield
Y - Al Lower Block
Z - Glass
Z'- Glass

Figure 3. A cross-section of the thermal conductivity apparatus.

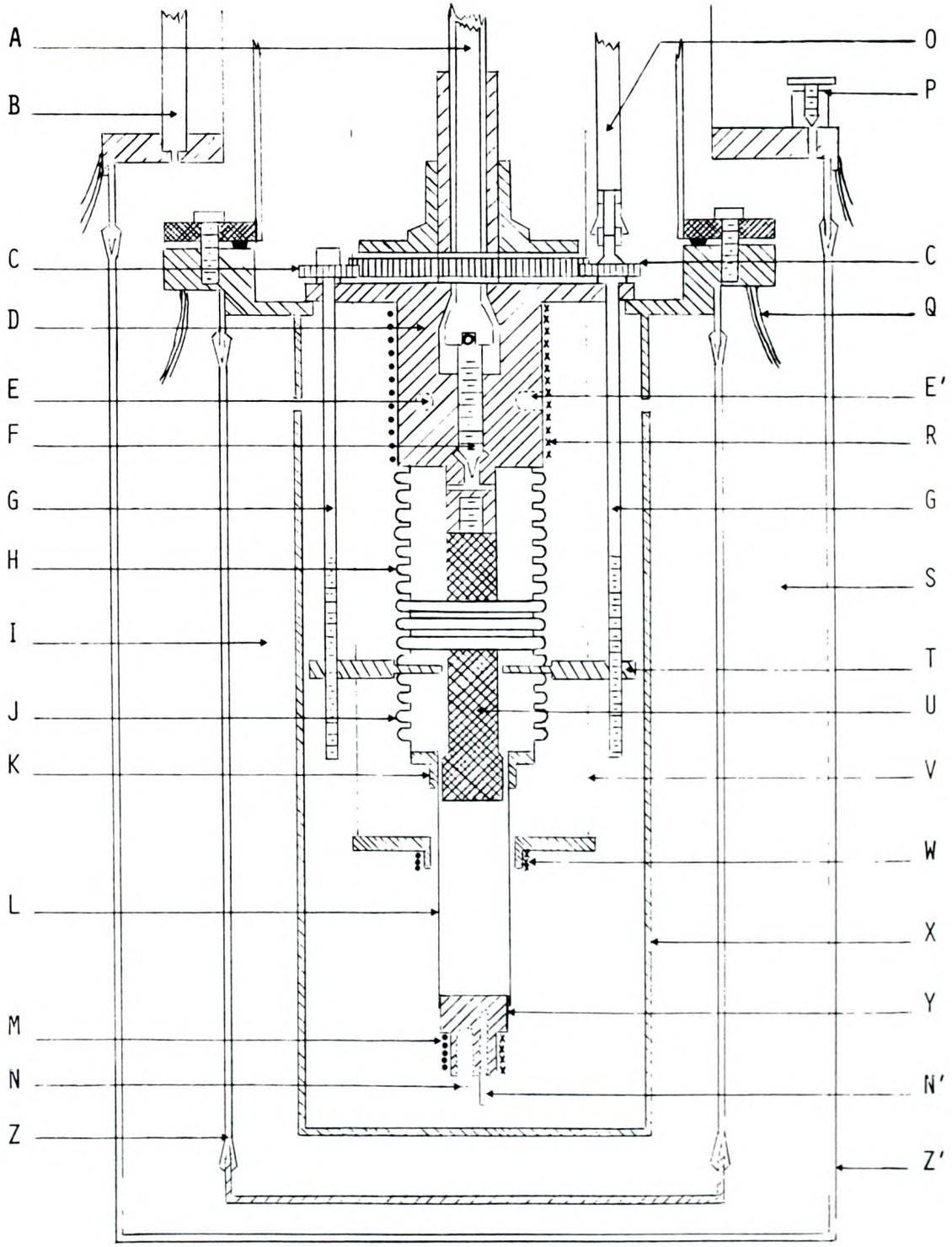
A
B
C
D
E
F
G
H
I
J
K
L
M
N
Z
O
P
C
Q
E'
R
G
S
T
U
V
W
X
Y
N'
Z'

Securing a leak-tight seal at the ends of the sample tube proved to be quite troublesome. Either the copper flange at the top or the Al block at the bottom, which were also secured with epoxy glue to the tube, developed leaks during several experimental runs. (This problem was due largely to the differences in thermal expansivity of the materials and the epoxy glue). This problem was later solved by increasing the bonding surface and by using a special low temperature epoxy glue (Stycast #2850 GT) which is ideally suited for low temperatures because of its low thermal expansivity and high thermal conductivity.

The sample tube is then secured by its copper flange with low melting temperature solder (Cerro-Bend) to the Cu lifting flange. The flange was employed to move the sample tube relative to a stationary Cu piston protruding into the sample tube. Furthermore, a short Cu bellows could also be installed between the lifting flange and the sample tube flange to enable us to measure the force exerted on the ends of the sample.

By varying the distance between the Cu piston and the Al lower block the sample chamber volume could be altered. This could be accomplished in one of two ways; either by replacing the Cu piston or by compressing (or expanding) the large Cu bellows soldered between the upper copper heat sink and the Cu lifting flange.

For the sample lengths of interest (0.3-3.0 cm) it was only necessary to change the length of the large Cu bellows.

This was accomplished by turning two long threaded brass rods screwed into two tapped holes in the Cu lifting flange. To keep the Cu piston and the sample tube aligned a set of brass gears soldered to the top of the rods and meshed to a third central gear served to synchronize the rotation of the rods.

To allow external control of the brass rods a thin-walled stainless steel tube was passed through a demountable O-ring seal at the top of the cryostat. An Allen wrench attached to the bottom of the stainless steel tube was used to turn an Allen cap screw soldered to the top of one of the brass rods.

To initiate crystal growth gaseous Ar was condensed directly into the sample chamber through the Ar needle valve in the upper block. This gas was supplied directly from a steel bottle through a stainless steel gas line and its pressure monitored by a Wallace and Tiernan pressure gauge.

An annular heater suspended around the sample tube aided in controlling the growth rate of the crystals. It consisted of a Cu ring wound with heater wire and was suspended from the top of the apparatus with cotton threads. (To allow external control the threads were tied to a pair of stainless steel tubes that exited through demountable O-ring seals at the top of the cryostat). The heater served to locally keep the sample slightly above the triple point and thus the growth rate of the sample was regulated by the rate at which the heater was raised.

To help maintain the sample at a constant temperature and to reduce heat loss by radiation a Cu radiation shield enclosed the sample chamber. The radiation shield was provided with long slits covered with transparent Mylar to allow visual examination of the sample. The introduction of helium exchange gas into the vacuum chamber (between the sample chamber and the exchange gas chamber) helped reduce the thermal gradients present during crystal growth and during the cool-down process. During thermal conductivity measurements this vacuum region was evacuated to approximately 10^{-7} Torr as measured by an ionization gauge. Aluminized Mylar glued onto the surface of the Cu radiation shield helped to further reduce heat loss by radiation to the surrounding cryogen.

The exchange gas chamber also served as a coarse temperature control by acting as a variable heat leak from the upper heat sink to the surrounding cryogen. For temperatures above 5 K this was accomplished by introducing an appropriate amount of helium exchange gas through the He gas inlet line. This pressure was monitored by two Wallace and Tiernan gauges at pressures above 1 Torr and by a Veeco thermo-couple gauge at pressures below 1 Torr. For temperatures below 5 K the chamber was filled with liquid He by siphoning it directly from the surrounding bath through the liquid He needle valve. To improve the heat exchange braided copper wire was soldered to the copper flange of the upper heat sink. This aided the exchange of heat by

presenting a large effective area to the He exchange gas. All of the common practices used to minimize heat conduction in cryogenic apparatus were employed in constructing the remainder of the apparatus. For example, all of the vacuum and gas lines of the cryostat were constructed of low thermal conductivity, thin-walled stainless steel tubing. In addition all of the electrical wires leading to the sample chamber were made of #36 gauge Cu wire and were thermally anchored to the He bath. This was accomplished by wrapping the wire several times around the Cu heat sinks in contact with the bath and then varnishing the wires in place.[33,34]

External to the cryostat the gas handling system (except for the Ar gas line) was constructed of Cu tubing. A pumping station was used to evacuate the system through a pumping manifold containing the necessary valves. This station consisted of a liquid N_2 trap, a diffusion pump and a rotary backing (and roughing) pump.

2. Temperature Control

For the duration of the experiment, especially during the thermal conductivity measurements, it is necessary to keep the sample chamber at a constant temperature. In principle this can be accomplished by controlling the rate at which heat is lost from the sample chamber to the cryogenic bath.

Throughout the temperature range of interest precise temperature control was obtained by employing a combination of different methods. A coarse temperature control was

maintained by changing the vapor pressure of the cryogenic bath and by carefully adjusting the exchange gas chamber pressure. The vapor pressure of the bath was controlled by pumping vapor of the cryogenic bath through a manostat type pressure regulator with a mechanical vacuum pump.[33] Using this procedure it was possible to regulate the temperature of the bath to within ±0.02 K for liquid N_2 and ±0.002 K for liquid He.[34] However, a drop in the bath level, the desorption of He atoms from the exchange gas chamber walls, etc., can alter the thermal loads at the upper heat sink and make it difficult to maintain the sample chamber itself within these limits.

This difficulty can easily be overcome and precise temperature control can be had by compensating for the change in thermal loads with an electronically controlled heater. The temperature controller employed for this experiment is a Model 5301 manufactured by Artronix Instrumentation Inc. (St. Louis, Missouri). Its principle of operation is briefly summarized in the paragraphs that follow and a block diagram is included in Figure 4.

The temperature controller monitors temperature deviations with an AC bridge and a phase sensitive detector in conjunction with a differential AC amplifier. One of the legs of the bridge consists of a temperature sensor (either a Ge or Pt resistance thermometer) secured in place with vacuum grease in a drilled cavity located in the upper Cu block. The other leg located on the front panel of the

T. S. - Temperature Sensor (Ge or Pt)

POT - 10 Turn Potentiometer (Temperature Set Point)

AMP_1 - Narrow Band Amplifier

AMP_2 - Differentiating Amplifier (Rate)

AMP_3 - Proportional Amplifier (Size)

AMP_4 - Integrating Amplifier (Duration)

DET - Phase Sensitive Detector

OSC - Oscillator

O. P. - Output Circuit

H - 120 Ω Heater Wire

S - Servo

O. POT. - Output 10 Turn Potentiometer (Power Output)

Figure 4. A block diagram of the Artronix temperature controller

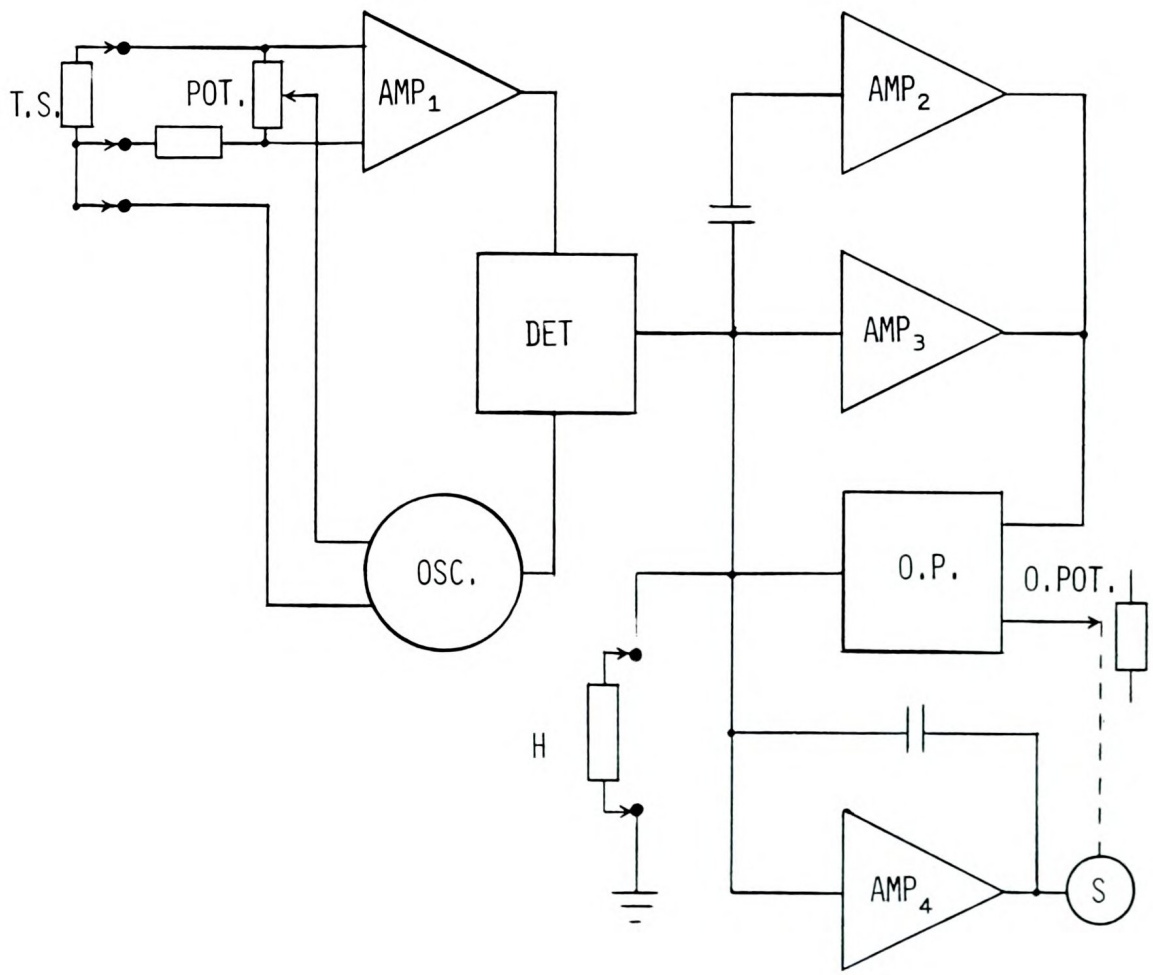
T.S.
POT.
AMP1
AMP2
DET
AMP3
OSC.
O.P.
O.POT.
H
AMP4
S

temperature controller is a variable ten-turn potentiometer that determines the temperature set point. A generator (or oscillator) provides a stable AC signal to both the bridge circuit and the phase sensitive detector and operation of the temperature controller is the result of comparison of the phase relationship of the input and output of the AC bridge.

During the bridge balance condition the potential drop across the temperature sensor and across the set point resistance are equal. Whenever the temperature of the upper block changes, the sensor resistance changes and the bridge is no longer in balance. The output signal from the bridge is then in or out of phase with the generator signal, depending on whether the temperature deviation is above or below the temperature set point. That is, the input voltages to the phase detector from the bridge circuit and the generator are either both of the same sign tending to be in phase or of the opposite sign tending to be out of phase.

The out-of-balance signal is then amplified by the AC differential amplifier and phase analyzed relative to the oscillator signal. The difference in phase is then used to produce a DC signal which is further amplified and fed into the output control section containing the heater wire which is wound about and varnished to the upper Cu block. The power delivered to the heater is adjusted continuously according to the size (proportional amp), duration (integrating amp) and rate (differentiating amp) of the

temperature deviation. Furthermore, by minimizing the power output requirements of the temperature controller it is possible to maximize the overall sensitivity of the system and thus maximize the temperature controllability of the sample chamber.

During the sample growth process the sample chamber temperature must be kept nearly constant for several days. This is accomplished by admitting an atmosphere of He exchange gas into the liquid helium dewar (inner dewar), admitting a few Torr of He into the exchange gas chamber, admitting 1 Torr in the vacuum chamber and maintaining the level of liquid N_2 in the outer dewar constant. The liquid N_2 level was maintained essentially constant by an automatic liquid N_2 filler system of 25 liter capacity that required refilling approximately every three days. In this way enough heat exchange between the sample chamber and the liquid N_2 bath was present to enable the temperature controller to maintain the sample chamber temperature close to the triple point of Ar. It should be noted that although the temperature control occurs at the upper Cu block the presence of the Cu radiation shield which is soldered to the upper block defines a thermal equipotential and the He exchange gas in the vacuum chamber maintains the sample chamber at a constant temperature.

To carry out thermal conductivity measurements in the high temperature region, liquid N_2 was transferred directly into the liquid He dewar (inner dewar). The liquid N_2 bath

temperature was kept constant by regulating its vapor pressure through a manostat and monitored with a Hg manometer while the sample chamber temperature was kept constant by the temperature controller. In order to extend this temperature range below 63 K (the triple point temperature of liquid N_2) the liquid N_2 was solidified by reducing its vapor pressure below its triple point pressure of 94 Torr and then regulating the sublimation pressure of the solid N_2. Enough cooling capacity was available to enable us to extend the temperature range down to 48 K by these means.

For obtaining temperatures below 48 K liquid He was transferred directly into the He dewar surrounding the thermal conductivity apparatus. The nature of the cooling process required that we first carry out measurements at the lowest temperatures from 5 K to 2 K. After cooling to 4.2 K liquid He was admitted via a He needle valve directly into the exchange gas chamber from the surrounding bath. Temperature control was accomplished by employing the same technique used for liquid N_2. Next, for temperatures above 5 K and below 48 K there is no convenient cryogenic liquid and it was necessary to continue using liquid He in this range. Between 5 K and 10 K it was necessary to pump out the liquid He from the exchange gas chamber and to reduce its pressure from 1 Torr to 10 mTorr as we slowly increased the temperature. Above 10 K it then became necessary to completely evacuate the exchange gas chamber, since more than sufficient thermal contact was present to require the

use of the temperature controller to raise the temperature of the sample chamber above 10 K.

Throughout the experiment the bath vapor pressure and the exchange gas pressure were judiciously adjusted to enable us to use the temperature controller at its maximum sensitivity. Use of this technique allowed us to achieve a constant temperature control to better than ±0.001 K at the lowest temperatures (2 K-10 K), ±0.005 K at the intermediate temperatures (10 K-40K) and ±0.01 K at the highest temperatures (40 K-83 K).

3. Temperature Measurement

The temperature and temperature gradient must be known precisely during the thermal conductivity measurements and during the sample growth process. To accomplish this calibrated Ge and Pt resistance thermometers (manufactured by Scientific Instruments, Lake Worth, Florida) were installed in the Al lower block. In the upper heat sink were installed initially uncalibrated Ge and Pt thermometers to serve as sensors. These Ge and Pt sensors are then calibrated against the thermometers located in the Al lower block. To insure that the thermometers and sensors are in good thermal contact all were imbedded in drilled cavities and secured in place with vacuum grease. To avoid falsely elevating the temperature of the thermometers due to thermal heat leaks from room temperature through the electrical leads all of the leads were made of #36 gauge copper wire and were thermally anchored to the upper heat sink.

To measure the resistance of the thermometers a four-leaded DC potentiometeric method was used. Two of the leads carried the excitation current which was 10 μamps below 34 K and 100 μamps above 34 K, while the remaining two were used to measure the potential drop across the thermometer. A Leeds and Northrup K-5 potentiometer and null detector system was used to standardize the excitation current and a Keithley 174 digital multimeter was used to measure the voltage drop across the thermometer and thus its resistance. The potential drop was actually measured twice-once with the excitation current flowing in the forward direction and again in the reverse direction. The two results were then averaged to cancel out the thermal emf's present. Figure 5 contains a schematic of the circuit used to measure the thermometer resistances and also included is the circuit for the lower Al block heater.

The calibration for the Ge resistance thermometer was provided in tabular form by the manufacturer, Scientific Instruments. This calibration was performed against a secondary N.B.S. Ge standard thermometer. Calibration points were provided for every 0.25 K for the lowest temperatures (1.5 K to 5.0 K), every 0.5 K to 2.0 K for the intermediate temperatures (5.0 K to 20 K), and every 5.0 K for the highest temperatures (40 K to 100 K). In order to interpolate for temperatures between these points the calibration data were fitted (for overlapping temperature intervals) to a quadratic equation of the form[33]

R_1 = 0-10KΩ

R_2 = 0-100KΩ

R_3 = 0-100KΩ

R_4 = 680-780KΩ

R_5 = 100Ω Precision

R_6 = 10Ω Precision

V_1 = 6 Volts

V_2 = 6 Volts

R_{Ge} = Germanium Thermometer

R_{Pt} = Platinum Thermometer

R_H = Lower Block Heater

Figure 5. A schematic diagram of the thermometer and lower Al block heater circuits.

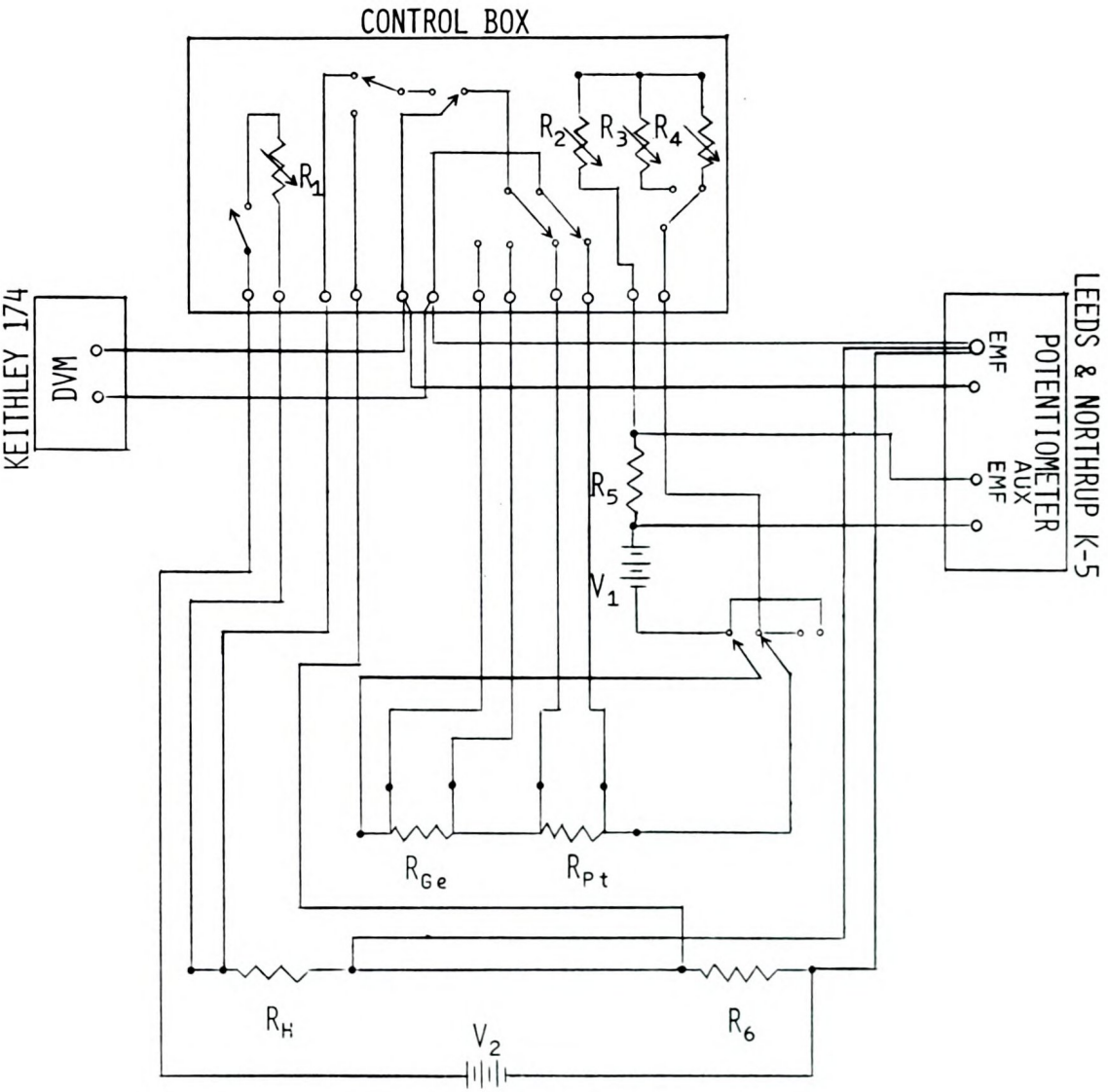
CONTROL BOX
R1
R2
R3
R4
KEITHLEY 174
DVM
LEEDS & NORTHRUP K-5
POTENTIOMETER
EMF
AUX
EMF
R5
V1
RGe
RPt
RH
R6
V2

$$1/T = a_0 + a_1 \ln R + a_2 (\ln R)^2 \qquad (12)$$

using the method of least squares. The set of constants a_0, a_1 and a_2 for each line segment were determined by using at least 5 calibration data points. Furthermore, the set of constants chosen were those that yielded line segments that were smoothly connected. The temperatures between 1.5 K and 50 K were calculated by using the above formula after substituting the appropriate constants and the measured value of the Ge thermometer resistance.

Since above 50 K Pt thermometers are more sensitive than Ge thermometers, all of the temperature measurements above 50 K were taken with the Pt thermometer. We calibrated this particular thermometer against another Pt thermometer (which had been calibrated by N.B.S.) by comparing the values of their resistances every single degree from 45 K to 90 K. The calibration data were then fitted for overlapping temperature intervals to a straight line of the form[33]

$$T = mR + b \qquad (13)$$

by the method of least squares. The set of constants m and b for each temperature interval were determined by using at least 10 points with one overlapping point at each end. By using the above formula and substituting the measured values of R along with the appropriate constants (m and b) the temperatures above 50 K could be determined.

The repeatability of the thermometers after thermal cycling between 4 K and room temperature is reputed by the

manufacturer, based on tests of the thermometers supplied, to be within ±0.5 mK. Our estimated accuracy of the temperature measurements, accounting for possible calibration errors, is no larger than ±2.5 mK in the 2-30 K temperature range and ±5.0 mK in the 30-90 K temperature range.

B. Sample Preparation

The technique chosen to grow the samples of Ar is similar to the technique used by Christen and Pollack[24] and previous workers.[27,35,36] Basically, it is a synthesis of the Bridgman and the zone melting techniques. That is, first a "seed" is grown from the melt and the rest of the crystal is directionally grown from bottom to top. A zone heater locally maintains the liquid above the growing sample at a temperature slightly above 83.8 K. This serves to control the rate of growth.

It has been found that employing this technique and growing the samples in a slow and even manner yield large-grained crystals of Ar. In fact, the grain size has been found to be inversely proportional to the growth rate.[37,38]

1. Sample Growth

Before cooling the apparatus to liquid N_2 temperatures to begin the sample growth process, all of the gas lines and vacuum regions were evacuated and flushed at room temperature. In particular, it is imperative that the Ar gas line and the sample chamber be charged with fresh Ar and evacuated several times to remove any contaminants or impurities present. After flushing the Ar line and the sample chamber a fresh

charge of Ar gas at approximately an atmosphere was admitted into this region.

To initiate the cool down process the outermost dewar was filled with liquid N_2. To speed up the cooling rate a "thumbfull" of air was admitted into the vacuum jacket of the liquid He dewar through a stopcock normally used to pump out this vacuum region. In addition He exchange gas was admitted into the other vacuum regions-1 atmosphere into the He dewar, 14 Torr into the exchange gas chamber and 1 Torr into the vacuum chamber.[34]

While the apparatus cooled we adjusted the position of the sample chamber so that the tip of the Cu piston protruded slightly into the sample chamber. When the sample chamber reached 79 K the pressure inside the (closed off) Ar gas line dropped below 300 Torr. We then slowly increased the Ar pressure to approximately 100 Torr above the triple point pressure of 516 Torr and liquid Ar was observed to readily condense into the sample chamber. Once the sample tube is filled with liquid (in approximately 30 minutes) the Ar inlet needle valve was closed. At the end of this time the sample chamber temperature had risen above 83.8 K. The sample was then allowed to cool down gradually to a few tenths of a degree above its triple point temperature of 83.8 K. The sample was then held at this temperature for about an hour to allow the liquid Ar to reach a uniform temperature.

Although care had been taken to decouple the apparatus

from mechanical vibrations transmitted through the floor, all unneeded vacuum pumps were turned off during the following phase of the sample growth process. This was done to minimize the possibility of inducing defects during this early phase.

To begin the seed growing phase the annular heater was lowered into place. It was positioned near the bottom of the sample chamber so that a 1-2 mm gap was visible between the top of the Al block and the bottom of the annular heater. To locally maintain the liquid inside the region of the annular heater above 83.8 K, 10 mwatts of power were delivered to the heater as the temperature set point, which controls the upper block temperature, was slowly reduced at the rate of 0.25 K/hr. The temperature was continuously lowered until a thin wafer of solid Ar of about 0.5 mm in thickness appeared at the Al lower block. The apparatus was then left in this steady state condition for a period of 12-24 hours.

During this annealing period it is expected that the larger crystal grains will absorb the smaller ones until a lower energy configuration is reached. This increases the likelihood that the wafer or seed will present itself as a single crystal to the melt (liquid Ar).

The remainder of the crystal was then grown by slowly raising the annular heater at the rate of 0.5 mm/hr. A driving mechanism situated outside and mounted above the apparatus served to raise and lower the heater. The driving

mechanism was essentially a winch powered through a reducing gear box coupled by a pair of demountable gears to a 1 and 2/3 r.p.m. synchronous motor. By replacing the driving gears with a pair having a different ratio or by replacing the synchronous motor with one of a different r.p.m., the rate of raising the annular heater could be altered.

Besides determining the rate of growth of the sample, the annular heater also served to inhibit the nucleation of additional crystals at the Mylar walls. Since the thermal conductivity of the solid Ar is considerably less than the thermal conductivity of the Mylar walls the heat of fusion would be easily conducted away through the Mylar walls if the annular heater was not present.

As the sample continued to grow a vapor space was observed to very slowly increase in size in the region between the solid Ar growing downward from the upper Cu piston and the upper surface of the Ar melt. The appearance of this gap is attributable to two of the many unusual properties of solid Ar. First, the density of solid Ar is 15% higher than the density of its liquid, so that approximately 13% of the sample chamber volume will be left vacant when all of the liquid within the sample chamber freezes. Second, the sublimation pressure of solid Ar near its triple point temperature is very high (516 Torr), so that the presence of a thermal gradient induces vapor phase mass migration from the slightly warmer sample tube to the cooler region near the Cu piston. Thus solid will tend to condense in

the free volume between the Cu piston and the large Cu bellows.

The presence of the vapor gap, unfortunately, provided ideal conditions for the appearance of vapor snakes,[39] an interesting phenomenon in itself. The growth process was momentarily halted on a few occasions when the sample chamber became filled with vapor snakes.

As the upper surface of the melt drops below 83.8 K a crust will freeze on top of the melt. The melt in the closed volume between the crust above and the solid below is now effectively sealed off. As more of the melt below the crust continues to solidify a vapor filled bubble appears just below the crust. As the size of the bubble continues to increase atoms from the surrounding liquid evaporate to fill the available volume. Due to argon's large heat of vaporization compared to its heat of fusion,[8] a solid shell will freeze around the bubble as Ar atoms on the liquid surrounding the bubble evaporate to the available vapor space. Further solidification of the liquid leads to more free volume and the bubble propagates into the melt as a vapor filled tube with a transparent thin-walled solid sheath.[8] If the vapor snake propagates beyond the annular heater and reaches the crystal's upper surface, it then becomes necessary to halt the growth process in order to melt the vapor snake.

This was accomplished by momentarily stopping the annular heater's ascent and increasing the power delivered

to it from 10 mwatt to 40 mwatt until the vapor snakes receded or melted. The power was then slowly decreased to a value slightly above 10 mwatt and we then resumed raising the annular heater. This procedure was necessary to prevent the nucleation of new crystallites.

For the longer samples studied (2.0-3.0 cm), after approximately two-thirds or more of the sample had grown, the amount of liquid present above the sample was insufficient to continue growing the sample from the melt. It thus became necessary to stop the growth process in order to condense more liquid Ar. This was accomplished by first gradually raising the temperature of the upper Cu block to 83.8 K and then admitting more Ar gas through the Ar needle valve until the vapor gap was filled with liquid. The temperature of the upper Cu block was then slowly reduced back down below 83.8 K and the growth process resumed.

When the sample had reached the approximate desired length the growth process was stopped and the power delivered to the annular heater was turned off. To allow visual examination of the entire sample the annular heater was lowered to the bottom of the sample chamber.

At the end of the growth process solid Ar usually froze in the space between the Cu piston and the Mylar tube; this bound the two together. In order to free the Mylar tube from the Cu piston (to allow relative vertical displacements of the sample tube), it was necessary first to raise the temperature of the upper Cu block slightly above 83.8 K.

The Mylar sample tube was then raised until the top of the sample was in intimate contact with the bottom surface of the Cu piston. The Ar was then frozen in contact with the Cu piston by quickly reducing the temperature of the upper Cu block slightly below 83.8 K.

To reduce the likelihood of the Mylar and/or the Cu bellows from binding to the Cu piston during the subsequent experiment, it was necessary to remove the excess solid Ar within this region. This was effected by gently pumping on the sample through the Ar inlet needle valve. The pumping rate was carefully adjusted so that the sublimation pressure was reduced no more than 10 Torr below the equilibrium sublimation pressure. After pumping for approximately an hour the solid Ar was observed to sublime quite readily from the region between the Mylar tube and the Cu piston. This sublimation process was stopped when the vapor gap between the top of the sample and the Cu piston had increased to approximately 0.1 mm.

To achieve thermal contact once again the sample was raised toward and gently pressed against the Cu piston. Since solid Ar is quite plastic at these temperatures, the force required to deform the top surface of the sample so that it conformed to the surface of the Cu piston was relatively small, less than 15 nt.

Although it would ordinarily be difficult to determine whether the entire surface area of the Cu piston was in contact with the sample, the transparency of solid Ar made this

determination quite simple. By viewing the top surface of the sample from below it was easy to observe when the two surfaces were in uniform contact. That is, when the surfaces are separated light is almost totally reflected from the Ar surface and thus the Cu is only slightly visible. As the Cu surface begins to make contact, light can be observed to be reflected from the Cu surface where the Cu and Ar are in good thermal contact.

The same procedure which we have just described was used to prepare the shorter samples (less than 2.0 cm), except that enough melt was present initially to grow the samples for their entire length without interruption. Furthermore, in spite of the interruptions the average growth rate for all of our samples was approximately 0.2-0.4 mm/hr. All of the samples were then gradually cooled down to 79 K at about 0.5 K/hr and allowed to anneal for 24 hours before measurements were begun.

2. Sample Manipulation

It has been demonstrated that the study of gross crystalline characteristics may be carried out without the use of X-ray techniques. In particular, it has been shown that solid Ar is ideally suited for thermal etching techniques to study grain size.[8,22,24,37] The grain boundaries of a polycrystalline sample of Ar can be easily revealed by gently pumping on the solid while the sample temperature is near 83.8 K.

The mechanism for thermal etching can be understood by noting that atoms between grain boundaries are on highly defective sites. These are more loosely bound than those on a true crystal face and are more easily evaporated. In addition, atoms forming a surface at these highly defective sites have a higher surface free energy than those on true crystal surfaces and thus tend to migrate away from the grain boundaries as the surface energy approaches a minimum. Thus, the resulting preferential evaporation and surface migration results in the appearance of etched lines along the grain boundary.

Since the manner in which we prepared the samples for thermal conductivity measurements at low temperatures inevitably results in etched samples, it was not necessary to perform a separate experiment to determine the grain size of our samples.

In order to carry out thermal conductivity measurements in the temperature range of 2 to 48 K, the samples were first separated from the sample tube and then rapidly cooled from 79 K to 4 K in less than an hour. Data were then obtained as we first cooled down to 2 K and then as we warmed up from 2 to 50 K.

It was hoped that, by separating the sample from the sample chamber walls (or boundaries) prior to the cool-down process, the thermal strains induced by the constraints of the sample chamber could be reduced. With the sample at 79 K the vapor pressure over the sample was reduced from an

initial value of 260 Torr to a final value of 250 Torr by pumping on the Ar sample through the Ar needle valve. To speed up this process the annular heater was used to locally warm up the lateral sides of the sample to induce preferential evaporation of Ar from the sample tube walls. That is, as we continued to pump on the sample the annular heater was supplied with 6 mwatts of power as it traversed the length of the sample (down and up once) at the rate of 2.4 cm/hr. As soon as the annular heater had completed its sweep the Ar inlet needle valve was closed and the power supplied to the annular heater was turned off. At this point we noticed that the sample was nearly completely separated from the sample chamber boundaries, including the thermal heat source and sink boundaries, and the lateral surface had the appearance of etched glass. We further noticed the absence of etch lines associated with grain boundaries, indicating that the samples studied were possibly single crystals.

As we mentioned earlier, all of the samples that we studied were cooled at a very fast rate. This was accomplished by first admitting 250 Torr of He exchange gas into the vacuum and exchange gas chambers in order to minimize the size of thermal gradients present during cool-down. Next, liquid He was transferred directly into the He dewar and as the temperature of the sample neared 4 K the vacuum chamber was pumped down to as low a pressure as possible.

The temperature at which we attempted to establish mechanical contact with the sample ends was determined by the type of study we wished to carry out. First, to study the effect on the effective (or measured) thermal conductance caused by varying the force exerted on the sample ends at constant temperature, we attempted to establish mechanical contact only after the sample had been cooled down to 4 K.

The results of this study indicated that in order to achieve good thermal contact, mechanical contact would have to be maintained throughout the cool-down procedure for the subsequent experiments devoted to measuring the thermal conductivity of Ar.

Due to the high vapor pressure of Ar the sample has a tendency to reattach itself to the Mylar walls during cool-down. It was also noticed that solid Ar tended to condense onto the Cu piston. For the first set of experiments these problems were obviated by continuing to pump on the sample while it cooled down to 4 K. Mechanical contact was then achieved at the desired temperature. Unfortunately, for these samples the combined effects of rapid pumping and cooling produced samples that were quite opaque.

For the second set of experiments we attempted to maximize the contact surface area at the sample ends by continuously pressing on them by raising the sample tube up to the Cu piston during the cool-down procedure. This procedure also prevented Ar from condensing from the vapor

state onto the Cu piston surface at the Cu-Ar interface. Since Ar is extremely plastic between 79 K and 54 K, maximum contact area is easily achieved. At 79 K a force of approximately 15.2 nt was required to achieve contact at the Cu-Ar interface. However, below 54 K Ar starts to become quite hard and brittle and hence will only be slightly deformed with the application of the same force as the temperature approaches 4 K. This means that as the sample volume decreases and atoms evaporate away from the Cu-Ar interface to cooler regions, it becomes necessary to continuously apply a larger force on the ends of the sample as it cools below 54 K up to a maximum of 30 nt at 10 K.

We should note at this point that the positive stress exerted on the Ar sample between 50 and 79 K causes the ordinarily cylindrical sample to bulge slightly and flow out towards the Mylar walls, reattaching the two once more. This is not unusual since carefully prepared samples of Ar have been observed to sag under their own weight.[40] This effect coupled with the atomic migration which causes recondensation between the Ar and Mylar tube walls firmly binds the sample to the sample tube once again. As we pressed and cooled these samples we heard a single "click" and noticed that the samples suddenly turned cloudy (but not opaque) at approximately 45 K. This phenomenon was probably due to the sample suddenly contracting away from the Mylar walls. Although some gross defects appeared near the ends and the middle of the largest samples, all of the samples

possessed a uniform cloudy appearance. Closer visual inspection of the samples revealed that the cloudiness appeared to be confined to the sample surface. We also observed that the smaller samples appeared less defective than the larger ones.

Since the thermal conductivity at temperatures above the thermal conductivity maximum is less dependent on crystalline quality, the precautions exercised in the low temperature experiments need not be observed for measurements between 48 K and 83 K. It was only necessary to separate the Mylar tube from the Cu piston prior to the measurements to allow relative motion of the Cu piston. Since the data were taken from 83 K down to 48 K, the sample on cooling tends to separate from the Al lower block. To obviate this difficulty we would press on the sample ends (in the same manner as was previously described) until thermal contact was reestablished.

3. Thermal Conductance Measurements

All of the thermal conductance measurements were performed in the same manner. With the vacuum chamber pumped out to the lowest vacuum possible and the upper Cu block maintained at a predetermined temperature T_u by the temperature controller, we first waited for the sample to reach a uniform temperature. At the lowest temperatures this time was of the order of seconds, while at the highest temperatures it was of the order of hours. The criterion for this initial steady state condition was that the thermometer at

the Al lower block had reached a constant temperature. This temperature was then recorded as the initial temperature T_i.

Next, joule heating was applied at a known rate to the lower Al block heater (See Figure 3). This heater was wired in a four leaded configuration to allow convenient potentiometric measurements of the voltage drop across it with the Keithley D.M.M. A 10Ω precision resistor wired in series with the heater was used to measure the current I delivered to the heater. The power $\dot{Q}_{App}$ delivered to the heater was then computed according to the relation $\dot{Q}_{App} = IV$.

After the sample had reached a steady state condition with a constant $\dot{Q}_{App}$ being delivered to the bottom of the sample this higher final temperature T_f of the thermometer at the Al lower block was also recorded. The temperature difference ΔT between the final and initial temperature was then computed, and the thermal conductance was calculated from the relation $K_{Eff} = \dot{Q}_{App}/\Delta T$. The temperature associated with K_{Eff} was taken to be the mean of the initial and final temperature.

That only one calibrated thermometer at the Al lower block is necessary to measure the effective thermal conductance can be easily demonstrated. Suppose that in the initial steady state condition ($\dot{Q}_{App} = 0$) that heat loss nonetheless occurs at the bottom of the sample. Then the rate at which heat is being supplied to the lower block is given by $\dot{Q}_i = K_{Eff}(T_u - T_i)$ where $T_u > T_i$. Now after the Al lower block heater is turned on in the final steady state

the net rate of heat conducted from the lower block to the upper block is given by

$$\dot{Q}_{Net} = \dot{Q}_{App} - \dot{Q}_i = K_{Eff}(T_f - T_u),$$

that is,

$$\dot{Q}_{App} = K_{Eff}(T_f - T_u) + \dot{Q}_i$$

Substituting for $\dot{Q}_i$ in the above expression we see that

$$\dot{Q}_{App} = K_{Eff}(T_f - T_i),$$

that is

$$K_{Eff} = K_{meas} = \dot{Q}_{App}/(T_f - T_i).$$

It can also be easily seen that the above result is also true for $T_u \leq T_i$.

To test for a possible dependence of K_{Eff} on ΔT we measured K for several values of ΔT. We observed no systematic dependence on ΔT. In general the ΔT's used were 0.02 K at the lowest temperatures near 2 K, 0.05 K near the thermal conductance maxima, 4-10 K, and 0.25 K near 83 K. These values were large enough to provide a small error in the measurement of ΔT, yet small enough so that the fractional difference between $K_{Eff}(\bar{T})$ and $K(T)$, the true thermal conductance, is much less than 1% (See Appendix D). The latter criterion is fulfilled when $\Delta T \leq 0.7$ at the lowest temperatures and $\Delta T \leq 28$ K at the highest.[14,25]

To investigate what effect pressing on the sample ends would have on the values measured for the thermal conductance, the short bellows was soldered in place between the sample tube flange and the Cu lifting flange (See Figure 3). To perform these measurements we started by first making

very light contact at the Cu-Ar interface. The thermal conductance was then measured as the applied force was increased while the temperature was kept constant. The applied force was determined by measuring the relative expansion of the bellows with a Wild cathetometer. The previously measured force versus bellows expansion was then used to determine the applied force.

A variation of the above experiments was conducted to determine the effect on the temperature dependence of the thermal conductance for a constant applied force at two different values. For this study and the subsequent ones the short copper bellows was removed. The first set of measurements was carried out after thermal contact was established at approximately 5 K. We then maximized the thermal conductance at this temperature by squeezing on the ends of the sample until we reached the maximum force that could be applied. Measurements of K_{Eff} were carried out for temperatures between 3-20K.

The temperature was then lowered back down to 5 K where the thermal contact was first broken and then re-established. However, in this case the force applied was such that K_{Eff} was approximately half the thermal conductance of the previous experiment at 5 K and measurements were then conducted over the same temperature range.

4. Thermal Conductivity Measurements

The results of the previous experiments indicated the presence of a thermal contact resistance that would have to

be determined in order to determine the thermal conductivty of the sample itself with the present apparatus. It was thus necessary to measure the thermal conductance as a function of temperature for samples of various lengths at the same thermal contact resistance.

Of course the ideal experiment would have been to measure K for various lengths of the same sample. We did attempt to follow this route. However, vacuum leaks in the sample tube limited the number of different lengths we could examine for the same sample. In spite of the difficulties we were able to measure K_{Eff} for two different lengths of the same sample for at least three different samples.

The procedure was to first measure K_{Eff} as a function of temperature for the longest sample. Next, the sample's temperature was raised to slightly above 83.8 K and the top of the sample was melted until the sample was the desired length. The excess Ar was then pumped out in the usual manner and the sample was allowed to anneal at 82 K until it regained its optical clarity. We then repeated the experiment for this next length.

The lengths of the samples were measured with the Wild cathetometer and their cross-sectional area was taken to be the same as the inner cross-sectional area of the Mylar sample tubes corrected for thermal expansion.

The thermal conductivity as well as the thermal boundary conductance was determined by fitting data to a straight

line of the form given by Equation (10) using the method of least squares.

III. EXPERIMENTAL RESULTS

A total of sixteen samples were grown to carry out our investigations. Table 1 contains a summary of the growth conditions for the samples that gave meaningful data. The average growth rate in Table 1 is defined as the length of the sample divided by the total time required to grow that length. For each of the first runs the annealing period is the time interval between the end of the growth period to the actual beginning of the first measurement of thermal conductance. For subsequent runs it is the time between the end of the previous run to the beginning of the next measurement of thermal conductance.

Samples 6, 7, and 10 were used to study the dependence of the thermal conductance on the force applied to the sample ends. Specifically, samples 6 and 7 were used to investigate the thermal conductance as a function of the applied force from 0.0 to 18.0 nt, while sample 10 was used to study the thermal conductance as a function of temperature for the two forces 15 nt and 30 nt. Samples 10, 11, 12, 13, 14, 15, and 16 were used to determine the thermal conductivity of solid Ar as a function of temperature from 2.2 to 83.0 K. We should further note that sample 15 was

used to carry out extensive thermal conductivity measurements in the high temperature range of 48 to 83 K.

Table 1

Summary of Sample Preparation

Sample No.	Run No.	Length (cm)	Ave. Growth Rate (mm/hr)	Annealing Time (Days)
6	2	0.86	0.20	5
6	3	0.67	0.20	2
7	2	1.72	0.34	2
7	3	0.83	0.34	1
10	1	1.57	0.34	1/2
10	2	1.17	0.34	2
11	3	1.97	0.26	1/2
11	5	1.34	0.26	6
12	1	2.84	0.31	4
13	1	0.33	0.36	0
13	3	0.95	0.28	2
14	1	3.00	0.25	4
14	2	2.98	0.25	4
15	1	1.28	0.19	1
16	1	0.63	0.25	2
16	2	2.41	0.37	1

A. Results of the Force Experiments

1. Measured Thermal Conductance versus Force

Table 2 contains the results of samples 6 and 7. Sample 6 run 4 consists of two sets of data for different but fixed temperatures one for 5.2 K and the other for 34 K. Sample 7 also consists of two sets of data, that is, runs 3 and 4. These are both for two different lengths approximately two to one in ratio taken at 9 K (See Table 1 for sample lengths).

The results of sample 10 run 1 are contained in Table 3 (See Appendix A). Included in this table are two sets of

data for the measured thermal conductance as a function of temperature for two different applied forces. Although the short Cu bellows (that allowed us to measure the applied force) had been removed for these and subsequent experiments, we can nonetheless estimate the two forces.

The applied force for the first set of data of Table 3 was approximately the maximum force we could apply 30 nt. The force for the second set of data of Table 3 was adjusted so that the thermal conductance at 5.0 K was approximately equal to one-half the thermal conductance at 5.0 K for the maximum applied force. To a first approximation the relationship between the thermal conductance and the applied force can be assumed to be linear, as we shall later show, so that the second force is approximately 15 nt.

2. Remarks on the Observed Effects of the Applied Force on the Measured Thermal Conductance

The data in Table 2 indicate that the measured thermal conductance increases as the applied force increases. This is expected since the area in contact at the Cu-Ar and Al-Ar interfaces increases, since the Ar will yield plastically at these interfaces as the force is increased. Since the yield stress of Cu and Al is 10^2-10^3 times greater than the yield stress of Ar throughout the temperature range studied, it can be safely assumed that Ar is the only material to plastically deform during these experiments. Berman[41] measured the yield stress of Cu at 4.2 K and found it to be 3.8 kbar, while Leonteva, et al.[42] found the yield

Table 2

Effective Thermal Conductance at Constant Temperature

Sample No. 6 Run No. 4

T = 5.2 K		T = 34.0 K	
Force(nt)	K_{Eff}(mw/K)	Force(nt)	K_{Eff}(mw/K)
0.0	0.12 ± 4%	0.0	1.62 ± 6%
3.6 ± 6%	0.75 ± 4%	3.6 ± 6%	4.60 ± 6%
7.9 ± 6%	1.70 ± 4%	7.9 ± 6%	5.18 ± 6%
17.5 ± 3%	2.29 ± 4%	13.3 ± 4%	5.85 ± 6%

Sample No. 7 T = 9.0 K

Run No. 3		Run No. 4	
Force(nt)	K_{Eff}(mw/K)	Force(nt)	K_{Eff}(mw/K)
0.0	0.12 ± 4%	0.0	0.43 ± 4%
0.8 ± 12%	0.33 ± 4%	0.6 ± 17%	3.75 ± 4%
1.7 ± 12%	7.56 ± 4%	1.4 ± 14%	5.13 ± 4%
3.6 ± 6%	9.89 ± 4%	2.1 ± 10%	6.79 ± 4%
5.6 ± 9%	13.07 ± 4%	2.9 ± 7%	7.37 ± 4%
7.9 ± 6%	13.84 ± 4%	6.2 ± 8%	11.12 ± 4%
13.1 ± 4%	14.92 ± 4%	7.2 ± 7%	12.10 ± 4%
		7.2 ± 7%	11.25 ± 4%

stress of polycrystalline samples of Ar to be 14.0 bar at 4.2 K.

That the Ar does indeed deform plastically at the surfaces can be made clearer by plotting the effective thermal resistance ($R_{Eff} = 1/K_{Eff}$) as a function of the reciprocal of the applied force (F^{-1}) for reasons which will be described below (See Equation (15)). The plots of these variables calculated from Table 2 are displayed on Figures 6 and 7. Although the data are sparse for sample 6 run 4, the 4 sets of data on Figures 6 and 7 clearly fit a straight line.

This behavior can be understood by noting that R_{Eff} consists of the thermal resistance of the crystal ($R = L/\kappa A$) in series with the thermal contact resistance ($R_{Cont} = 1/K_{Cont}$) at the two interfaces (Al-Ar and Cu-Ar). That is,

$$R_{Eff} = R + R_{Cont} \tag{14}$$

but

$$R_{Eff} = R + CF^{-1} \tag{15}$$

where C is just some proportionality constant.

Since on a microscopic level the ends of the sample are quite rough, we expect that the contact area will increase since the surface asperities deform readily while the force is increased. We can thus conclude that the thermal contact conductance at the interfaces is proportional to the applied force, that is, $K_{Cont} \propto F$.

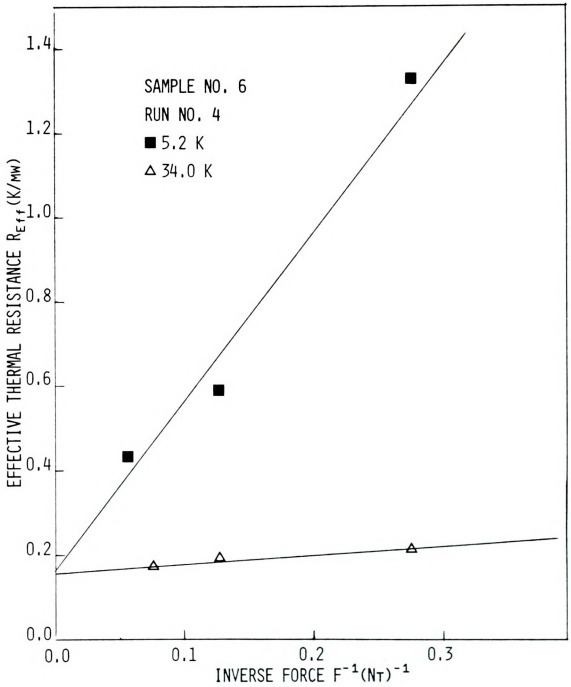

Figure 6. A plot of the effective thermal resistance of sample 6 as a function of the reciprocal of the applied force.

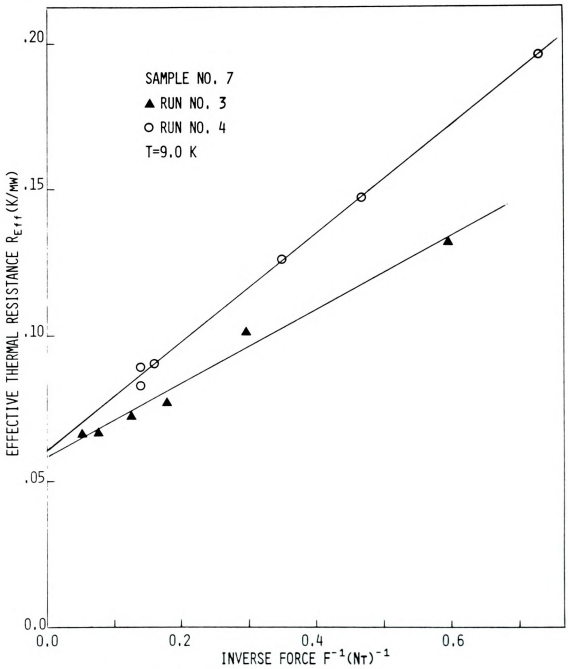

Figure 7. A plot of the effective thermal resistance of sample 7 as a function of the reciprocal of the applied force.

This result is in agreement with the experiments of Berman,[41] Berman and Mate,[43] and Mate[44] who measured the thermal contact conductance between pressed surfaces of various materials (Cu-Cu, Cu-diamond, Au-Au, sapphire-sapphire) as a function of the applied force at liquid He temperatures and observed an almost linear dependence.

An approximate relationship between K_{Cont} and F can be obtained by considering the following simplified picture of the surfaces. Assume that the average sized asperity is contained within a cube of side d, then the total boundary conductance of n asperities in contact (which can be considered to be in parallel) is given by

$$K_{Cont} = n\kappa d \tag{16}$$

where κ is the thermal conductivity of the material of the individual asperities. The total surface area A in contact is determined by yield stress P_c of the material and the force applied F. That is, as force is applied the asperities will continue to deform plastically until the ratio $F/A = P_c$ the yield stress. That is $A = F/P_c = nd^2$ so that

$$d = (F/nP_c)^{\frac{1}{2}}. \tag{17}$$

Substituting this result in Equation (16) yields that

$$K_{Cont} = (nF/P_c)^{\frac{1}{2}}\kappa. \tag{18}$$

Tabor has shown that for two steel surfaces in contact $n \propto F^{\frac{1}{2}}$, hence $K_{Cont} \propto F^{3/4}$, which is in approximate agreement with our results. Tabor has also shown that $K_{Cont} \propto F^{0.6}$ for deformations that take place elastically.[45]

In Figure 8 we show the data plotted from Table 3 (open circles, filled circles and filled triangles) including the data from sample 10 run 2 (filled squares). The two sets of data from Table 3 (open and filled circles) display essentially the same qualitative behavior, except that the maximum of $K_{Eff}(T)$ has been shifted. The shift of the peak toward a higher temperature for the smaller applied force (filled circles) is probably due to the increased dominance of R_{Cont} over R.

Curiously, below the peak the two lower sets of data (open and filled circles) in Figure 8 have a definite T^2 dependence, while the data of sample 10 run 2 (filled squares) have a temperature dependence somewhat less than T^2. It should be recalled that for sample 10 run 2 we attempted to maintain thermal contact with the crystal ends during the cooldown process. Although better thermal contact is achieved as is evidenced by the almost two-fold increase in the effective thermal conductance near the peak for run 2 (filled squares) over run 1 (open circles), it is unfortunately accomplished at the expense of the quality of the sample. Although some deformation of the entire sample is expected, severe deformation is probably confined to the sample ends. However this may be an irrelevant point since the samples are thermally strained 1% or more during cooldown. Even a strain this small is large enough to induce plastic deformation above 65 K.[42]

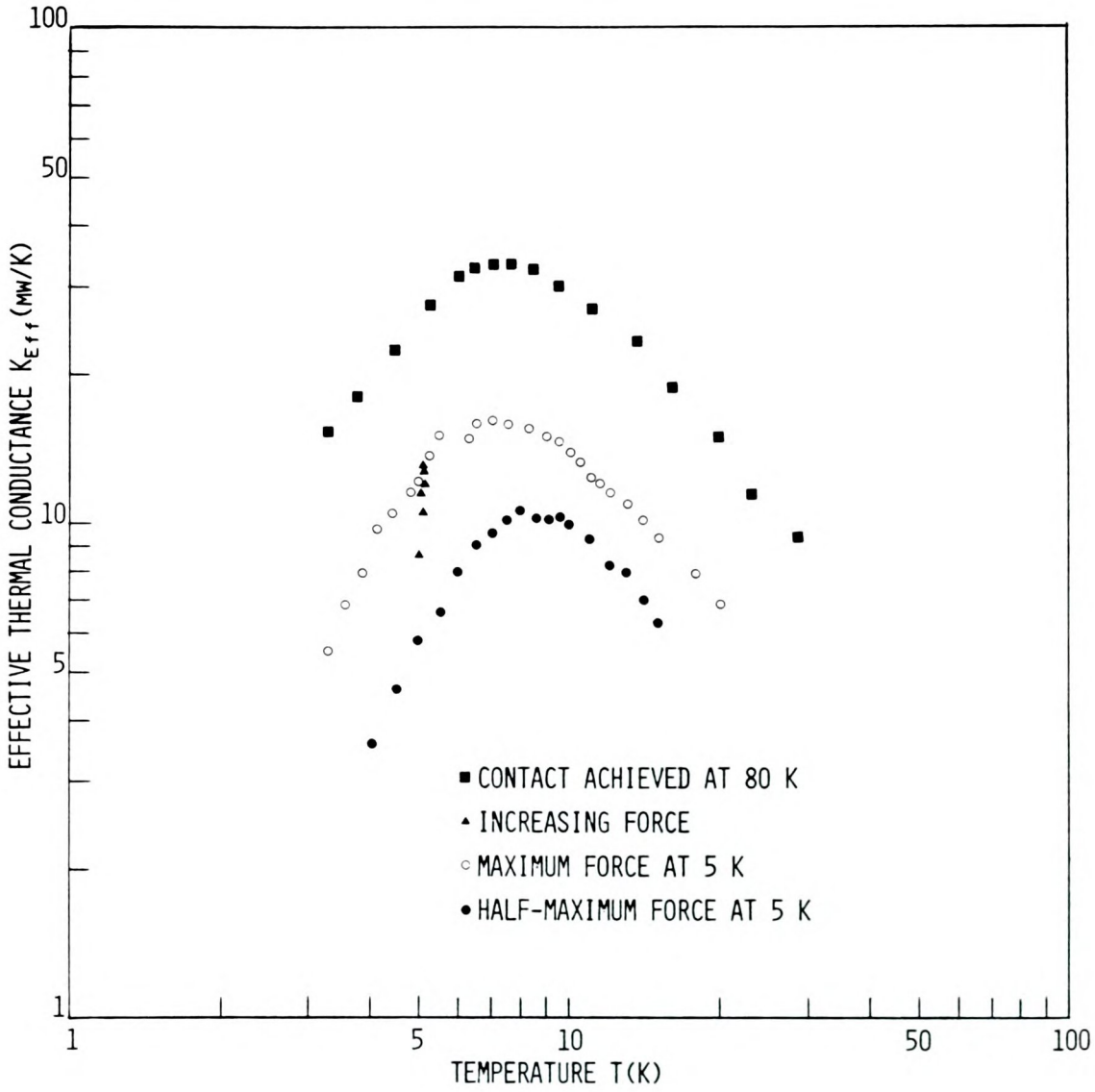

Figure 8. A plot of the effective thermal conductance for different methods of making mechanical contact.

3. Force Experiment Errors

The error in measuring the applied force F is due principally to the hysteresis associated with the non-elastic behavior of the small Cu bellows when large forces are applied. In a separate experiment this bellows was calibrated at 77 K by pressurizing its interior with He gas. The applied force F was determined from the applied over pressure and the cross-sectional area of the bellows (1.13 cm^2). Its extension was then measured as the force (pressure) was increased from zero to a maximum of 21 nt (1390 Torr) and then decreased to zero. Since these measurements yielded two sets of curves, the calibration curve was taken to be the mean of these two measured curves. Thus the maximum error in measuring the applied force F due to the inelastic behavior of the bellows was determined to be ±0.1 to ±0.2 nt for applied forces between 0.0 and 5.0 nt and ±0.5 nt for forces between 5.0 nt and above. The percentage error varied from 17% for the smallest applied force to 3% for the largest applied force. The error in measuring the absolute temperature T is due principally to the limits on our ability to keep the sample temperature constant (See Chapter II, Section 2). We estimate that the maximum error in measuring T (δT) is then ±0.001 K for 2 K$\leq$T<10 K, ±0.005 K for 10 K$\leq$T<40 K, and ±0.010 K for 40 K$\leq$T$\leq$83 K.

Since we were able to measure $\dot{Q}$ to better than 0.1% the largest source of error introduced in determining K_{Eff}

is in measuring ΔT. The maximum error that ΔT will introduce is twice the maximum error in T ($2\delta T$). The ΔT's used varied from 0.05 K near 4 K to 0.25K near 80 K. We estimate from these values that the maximum percent error in K_{Eff} varies from 4% at 4 K to 8% at 80 K.

B. Results of the Thermal Conductance Measurements

Table 4 in Appendix B contains all the measured thermal conductance values and their corresponding temperatures for samples 10-16. These samples were used to determine κ. The data presented in this table satisfy two experimental criteria.

First, the sample tube remained reasonably leak tight during the experimental run. That is, the sample did not gradually leak out of the sample tube into the surrounding vacuum region over a 24 hour period. A gross leak of this size could be easily verified by the inability of the vacuum pumping system to reduce the vacuum chamber pressure below 10 mTorr.

Second, mechanical contact with the sample was maintained throughout the cooldown process. That is, it should have been possible to continuously remove the slack on the lifting screw due to the contraction and sublimation of the sample. If the sample tube and the Cu piston remained frozen together for more than 15 minutes, we assumed that the mechanical contact had been lost.

Any data that did not meet these two criteria were discarded.

1. Thermal Resistance versus Sample Length

As suggested earlier, in the Introduction, the simplest model for the effective thermal resistance is two thermal resistances in series. One of these is due to the imperfect contact achieved at the sample ends $R_{Cont} = K_{Cont}^{-1}$. The other thermal resistance is due to the presence of the Ar sample which may be written, by definition, $R = L/\kappa A$ (L = length of the sample and A = cross-sectional area of the sample). Recalling Equation (10), this is expressed as

$$1/K_{Eff} = L/\kappa A + 1/K_{Cont} \cdot \qquad (10)$$

In order to determine whether the above relation is reasonably represented by our data, we must know K_{Eff} for each L at exactly the same temperature for the temperature range investigated. Since it is not feasible to measure K_{Eff} at exactly the same temperature for each L, we drew the smoothest curve through the raw $K_{Eff}(T)$ data for each length to interpolate and extrapolate for K_{Eff} at convenient temperatures. The values of $K_{Eff}(L)$ for these temperatures were determined graphically and are contained in Table 5 along with the corresponding temperature.

2. Calculation of the Thermal Conductivity

Figures 9 and 10 are plots of R_{Eff} as a function of L (length) at constant temperature for various isotherms from 2.25 K to 26 K. It is apparent from Figure 9 that below 3.5 K the longer samples show a greater scatter than the shorter samples. However as the temperature increases above 3.5 K the scatter diminishes and the data approach

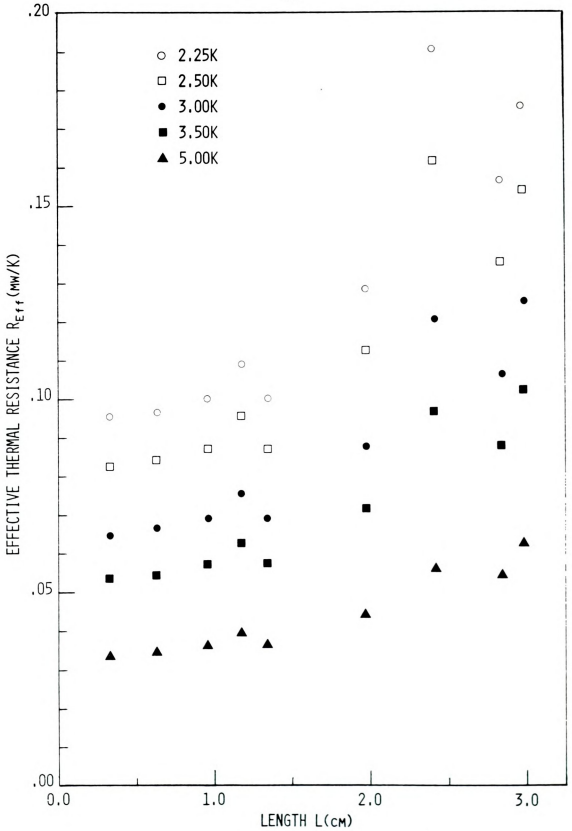

Figure 9. A plot of the effective thermal conductance versus sample length for several isotherms between 2.25 and 5.00 K.

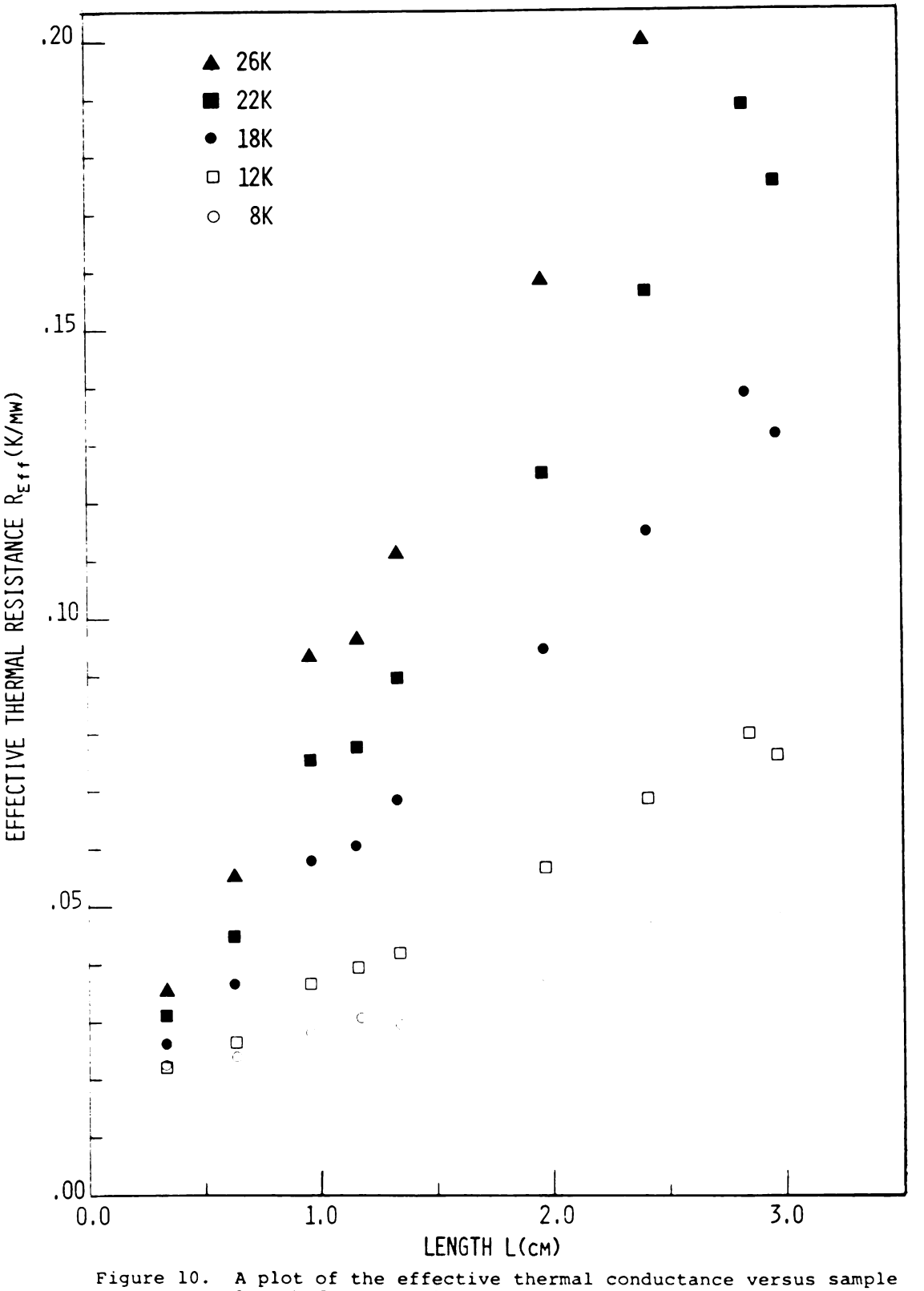

Figure 10. A plot of the effective thermal conductance versus sample length for several isotherms between 8 and 26 K.

very nice straight lines.

Since the samples were grown and manipulated in essentially the same manner, we assume that κ (thermal conductivity) and K_{Cont} (thermal contact conductance) are the same for each sample at the same force. Thus, in order to determine these two quantities we fit the data of Table 5 using the linear regression method to a straight line of the form

$$R_{Eff} = mL + R_{Cont} \tag{19}$$

where $\kappa = (mA)^{-1}$ and $K_{Cont} = R_{Cont}^{-1}$. The results of these calculations along with the correlation coefficients are contained in Table 6. A plot of the thermal conductivity $\kappa(T)$ is contained in Figure 11 along with the data of Clayton and Batchelder[23] and Krupskii and Manzhelii[20,21] for comparison. Above 65 K our plotted thermal conductivity values in Figure 11 are those obtained from Table 5 for sample 15 run 1.

Before we present the high temperature data in row form, we mention three interesting effects displayed by the raw data contained in Table 4. The three effects we are considering are as follows: (a) the dominance of $R_{Cont}(T)$ for the shorter samples ($L \leq 1.34$ cm) at low temperatures ($T \leq 6$ K), (b) the broadening and shifting of the maximum of $K_{Eff}(T)$ due again to presence of $K_{Cont}(T)$ and (c) the dominance of K at the higher temperature ($T \geq 38$ K).

It is clear by comparing columns 2-5 in Table 5 with column 3 in Table 6, for temperatures below 6 K, that the K_{Eff} is very nearly equal to the thermal contact conductance.

Table 5

Smoothed K_{Eff}(mw/K) Values

T(K)	$K_{Eff,1}$	$K_{Eff,2}$	$K_{Eff,3}$	$K_{Eff,4}$	$K_{Eff,5}$	$K_{Eff,6}$	$K_{Eff,7}$	$K_{Eff,8}$	$K_{Eff,9}$
2.25	10.5†	10.4†	10.0	9.2†	10.0†	7.8†	5.25†	6.40	5.70
2.50	12.1	11.9	11.5	10.5†	11.5†	8.9†	6.20	7.40	6.50
2.75	13.7	13.5	13.0	11.9†	13.0	10.1†	7.20	8.40	7.30
3.00	15.4	15.0	14.5	13.3†	14.5	11.4	8.30	9.40	8.00
3.50	18.8	18.4	17.5	16.0	17.5	14.0	10.4	11.4	9.80
4.00	22.5	21.8	20.7	19.1	20.7	16.9	12.8	13.6	11.7
4.50	26.2	25.4	24.0	22.1	24.0	19.7	15.3	16.0	13.7
5.00	30.0	29.0	27.6	25.4	27.6	22.8	17.9	18.4	16.0
5.50	33.8	32.2	30.3	28.5	30.0	25.2	20.0	20.3	18.2
6.00	37.0	35.0	32.5	31.0	32.0	26.2	21.5	21.7	19.8
6.50	39.4	37.5	34.0	32.3	33.5	27.0	21.8	22.3	20.8
7.00	41.7	39.4	35.3	33.0	34.2	27.4	22.4	22.4	21.3
7.50	43.6	41.0	35.9	33.2	34.2	27.1	22.3	22.0	21.4
8.00	45.0	42.0	36.0	33.0	33.8	26.5	21.7	21.2	21.0
8.50	46.2	42.2	35.3	32.5	32.9	25.5	20.9	19.9	20.0
9.00	46.8	42.0	34.3	31.6	31.5	24.4	19.8	18.6	18.8
9.50	47.0	41.4	33.4	30.4	30.0	23.4	18.8	17.5	17.7
10.00	47.0	40.6	32.0	29.5	28.5	22.2	17.5	16.3	16.7
11.00	47.2	39.5	29.7	27.5	26.5	20.0	16.2	14.2	14.7
12.00	46.9	38.1	27.5	25.4	24.2	17.8	14.6	12.6	13.2
14.00	44.6	34.6	23.4	22.0	20.2	15.0	12.0	10.2	10.8
16.00	41.2	30.5	20.0	19.3	16.6	12.5	10.1	8.50	9.10
18.00	38.0	27.4	17.3	16.6	14.6	10.6	8.7	7.20	7.60
20.00	35.0	24.8	15.0	14.6	12.7	9.1	7.4	6.15	6.50
22.00	32.2	22.4	13.3	12.9	11.2	8.00	6.40	5.30	5.70

Table 5 (cont'd)

T(K)	$K_{Eff,1}$	$K_{Eff,2}$	$K_{Eff,3}$	$K_{Eff,4}$	$K_{Eff,5}$	$K_{Eff,6}$	$K_{Eff,7}$	$K_{Eff,8}$	$K_{Eff,9}$	$K_{Eff,10}$
24.00	29.6	19.6	11.7	11.5	9.90	7.00†	5.60	4.65	5.00†	
26.00	28.0	18.2	10.7	10.4	9.00	6.30†	5.00	4.13	4.42†	
28.00	25.5	16.5	9.90	9.50†	8.20	5.70†	4.50	3.69	3.60†	
30.00	24.2	15.3	9.00	8.70†	7.50	5.20†	4.00	3.33	3.26†	
32.00	22.6	14.0	8.30		6.80		3.65	3.00	2.97†	
34.00	21.5	12.8	7.70†		6.30		3.32	2.75	2.70†	
36.00	20.0	11.9	7.10†		5.80		3.06	2.51		
38.00	18.95	10.95	6.55†		5.35		2.79	2.25		
40.00	17.95	11.0	6.15†		5.05		2.58	2.08		
42.00	16.9	10.45	5.74†		4.69		2.39			
46.00	15.3	9.94			4.13					4.33
50.00	13.93	8.83†			3.68					3.86
55.00	12.32	7.93†			3.22					3.14
60.00	11.01				2.86					2.81
65.00	9.90†				2.55					2.40
70.00										2.12
75.00										1.84
80.00										1.78

$K_{Eff,n}$ n =	1	2	3	4	5	6	7	8	9	10
L(cm)	0.33	0.63	0.95	1.17	1.34	1.97	2.41	2.84	2.98	1.28

† Extrapolated values

Table 6

Calculated Thermal Conductivity and Thermal Contact Conductance

T(K)	κ(mw/cmK)	K_{Cont}(mw/K)	Correlation Coefficient	K_{Cont}/κ(cm)
2.25	33.4 ± 22%	13.9 ± 20%	0.900	0.42
2.50	38.9 ± 23%	15.9 ± 21%	0.912	0.41
2.75	44.4 ± 23%	18.0 ± 20%	0.922	0.41
3.00	49.7 ± 21%	20.2 ± 18%	0.931	0.41
3.50	61.9 ± 20%	24.4 ± 17%	0.941	0.39
4.00	75.6 ± 17%	28.8 ± 14%	0.948	0.38
4.50	90.8 ± 17%	33.1 ± 14%	0.951	0.36
5.00	107.9 ± 17%	37.5 ± 13%	0.954	0.35
5.50	122.1 ± 16%	41.3 ± 11%	0.966	0.34
6.00	129.4 ± 12%	44.8 ± 9%	0.977	0.35
6.50	128.9 ± 12%	48.1 ± 10%	0.977	0.37
7.00	126.3 ± 12%	51.0 ± 10%	0.984	0.40
7.50	119.8 ± 12%	53.7 ± 11%	0.988	0.45
8.00	110.6 ± 11%	56.3 ± 12%	0.989	0.51
8.50	99.2 ± 10%	59.1 ± 12%	0.992	0.60
9.00	89.0 ± 9%	61.5 ± 13%	0.993	0.69
9.50	80.8 ± 8%	63.1 ± 13%	0.994	0.78
10.00	73.1 ± 7%	64.8 ± 13%	0.993	0.89
11.00	61.0 ± 6%	70.3 ± 14%	0.995	1.15
12.00	52.3 ± 5%	73.8 ± 15%	0.995	1.41
14.00	40.6 ± 4%	78.7 ± 16%	0.994	1.94
16.00	33.2 ± 4%	76.3 ± 16%	0.994	2.30
18.00	27.4 ± 4%	79.1 ± 22%	0.995	2.88
20.00	23.0 ± 4%	82.1 ± 22%	0.995	3.58
22.00	19.7 ± 3%	84.8 ± 23%	0.994	4.31
24.00	17.1 ± 3%	81.0 ± 22%	0.994	4.73
26.00	15.1 ± 3%	96.0 ± 26%	0.994	6.40
28.00	12.7 ± 3%	211.3 ± 57%	0.997	16.69
30.00	11.3 ± 3%	353.3 ± 96%	0.997	31.21
32.00	10.2 ± 2%	221.6 ± 48%	0.999	21.68
34.00	9.27 ± 2%	356.9 ± 77%	0.999	38.50
36.00	8.39 ± 2%	1504.7 >± 100%	0.998	179.30
38.00	7.58 ± 2%	666.6 >± 100%	0.998	87.94
40.00	6.86 ± 2%	-114.0 >± 100%	0.997	$>10^2$
42.00	6.65 ± 2%	-236.5 >± 100%	0.996	$>10^2$
46.00	6.38 ± 2%	-469.7 >± 100%	0.996	$>10^2$
50.00	5.65 ± 2%	-275.3 >± 100%	0.997	$>10^2$
55.00	4.67 ± 2%	+276.8 >± 100%	0.992	$>10^2$
60.00	4.33 ± 2%	274.2 >± 100%	0.997	$>10^2$
65.00	3.75 ± 2%	1213.9 >± 100%	0.992	$>10^2$

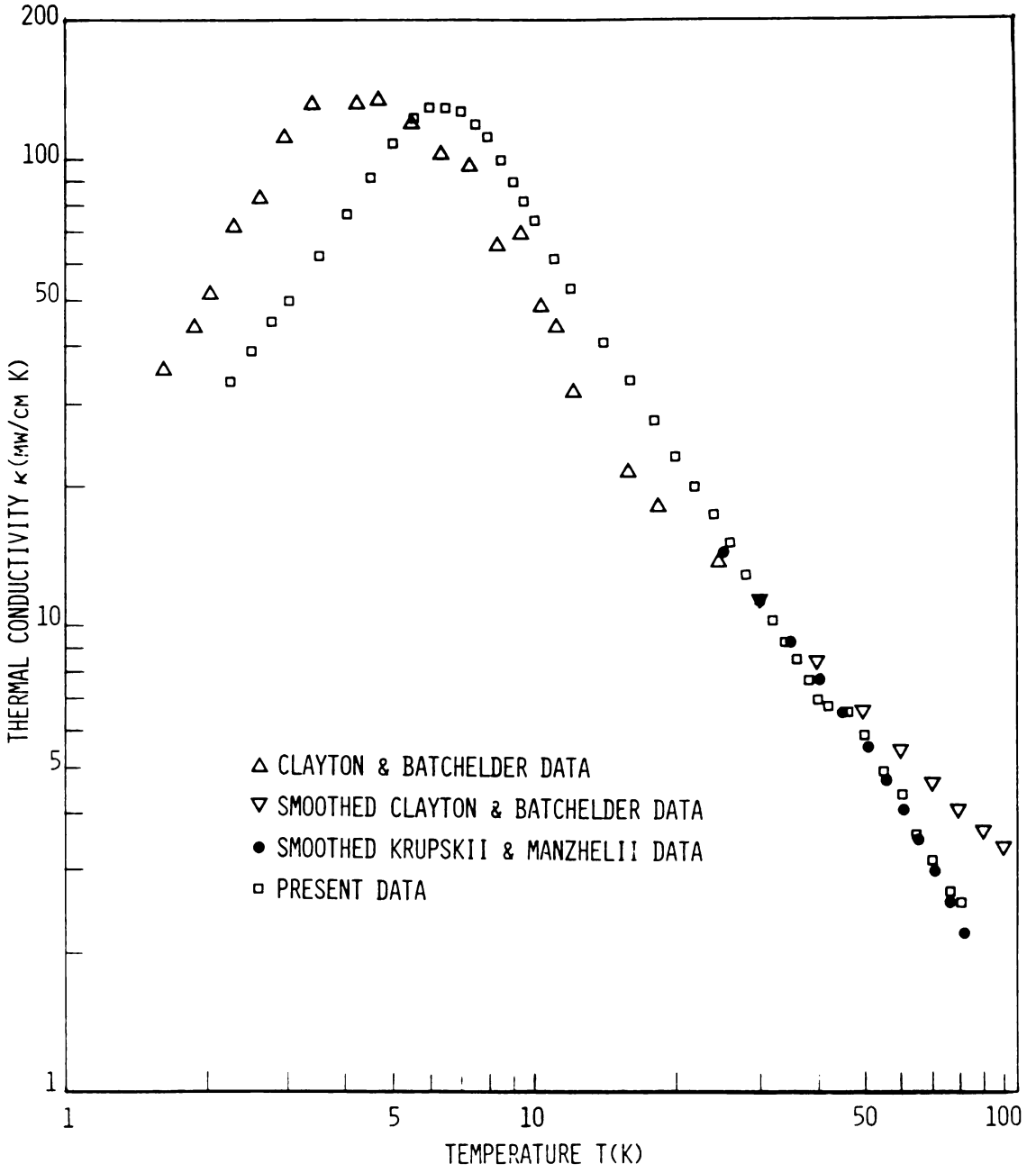

Figure 11. A plot of the thermal conductivity versus temperature. Included for comparison are the data of Clayton and Batchelder and Krupskii and Manzhelii.

For example, at 2.25 K, $(R_{Cont}/R_{Eff})(100\%)$ varies from 77% to 42% for the shortest to the longest sample. To illustrate this effect more clearly we show in Figure 12 plots of the effective (or measured) thermal conductance $K_{Eff}(T)$ for samples of various lengths. Below 6 K the data converge to K_{Cont} as the samples become smaller in length.

Figure 12 also illustrates the second feature, that is, as the samples become shorter the maximum of K_{Eff} is broadened and shifted toward higher temperatures. We expect that as $L \to 0$, $K_{Eff} \to K_{Cont}$. That this is approximately correct can be seen by comparing Figure 12 with Figure 13 which contains a plot of $K_{Cont}(T)$ taken from the data of Table 6. Between 2 and 20 K it can be seen that $K_{Eff}(T)$ does indeed approach $K_{Cont}(T)$ as L becomes shorter. (Above 20 K the behavior of $K_{Cont}(T)$ is slightly more complicated. We shall discuss this later.)

The third feature is that above 38 K the conductance of the sample is now dominant. For example at 38 K (R_{Cont}/R_{Eff}) (100%) varies from 2.8% to 0.3% from the smallest to the largest sample. To further illustrate this effect in Figure 14 we plot $K_{Eff}(L/A)$, the effective thermal conductivity, as a function of temperature for several sample lengths.

In view of this last effect we can safely assume that above 38 K the measurements we have carried out have yielded $\kappa(T)$ directly. In Figure 15 we plot the raw thermal conductivity data (corrected for K_{sp} the spurious heat conductance due to the mylar tube, wire leads, etc.) of Table 7.

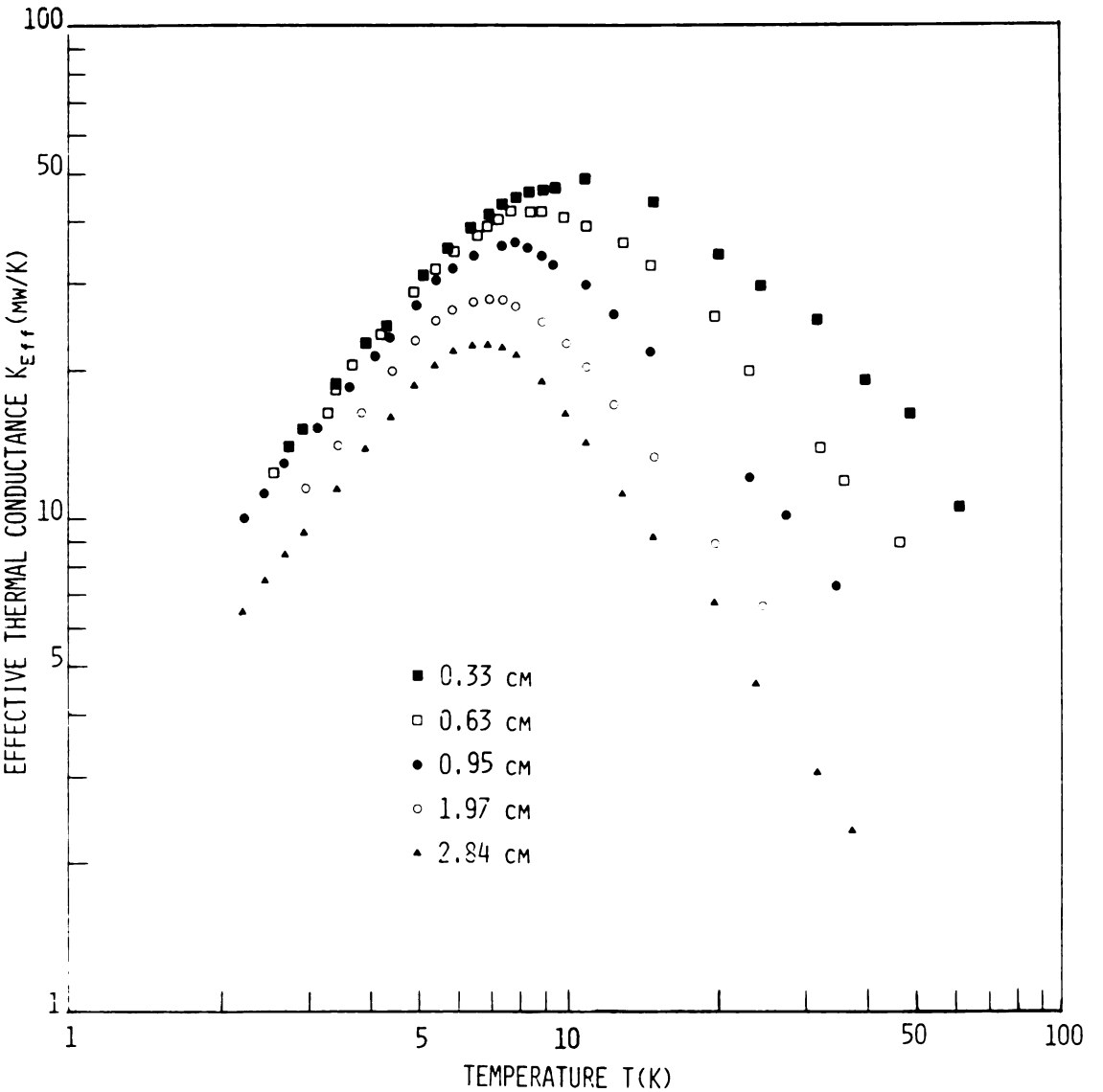

Figure 12. A plot of the effective thermal conductance versus temperature for samples of different lengths.

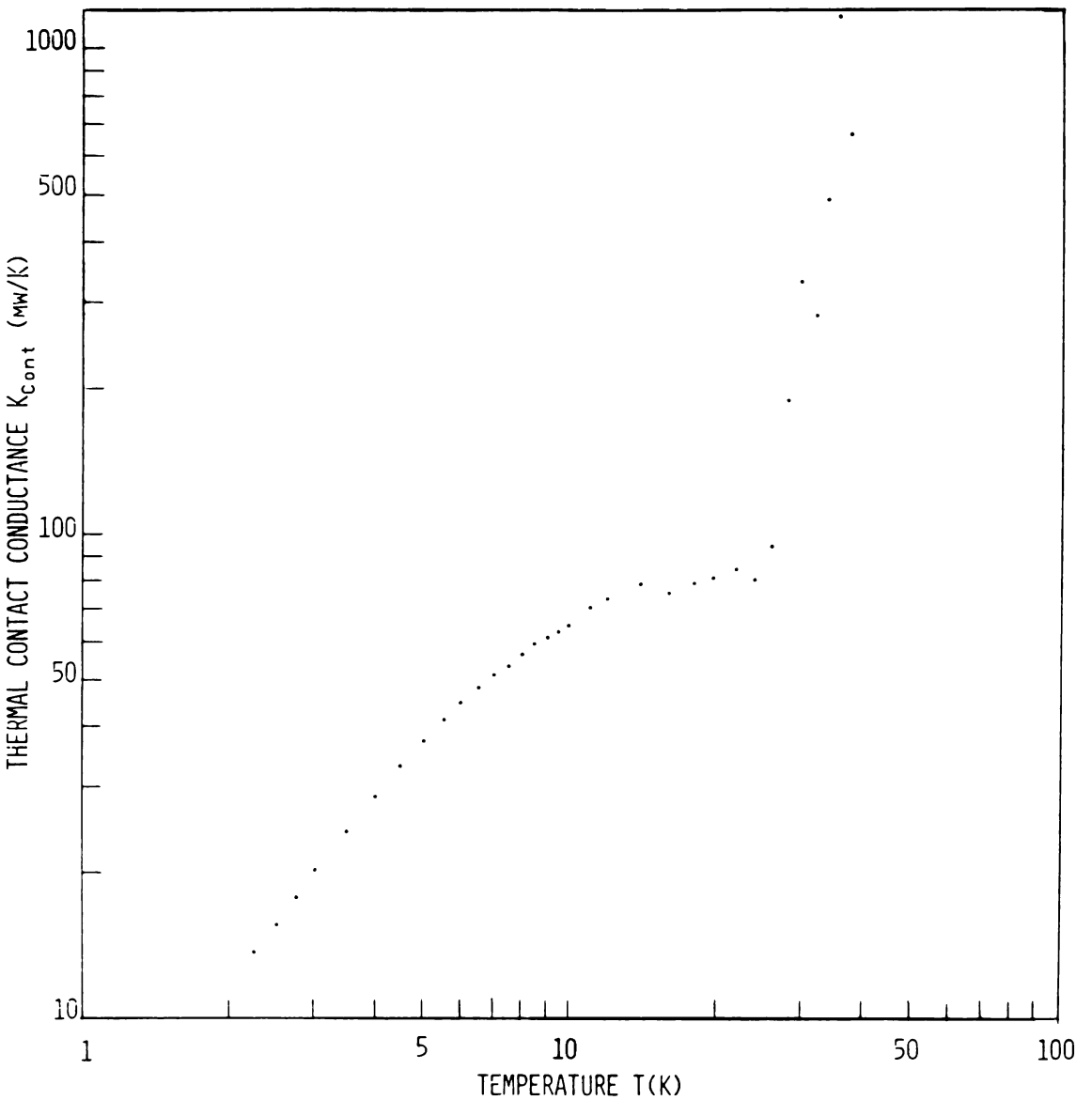

Figure 13. A plot of the thermal contact conductance versus temperature.

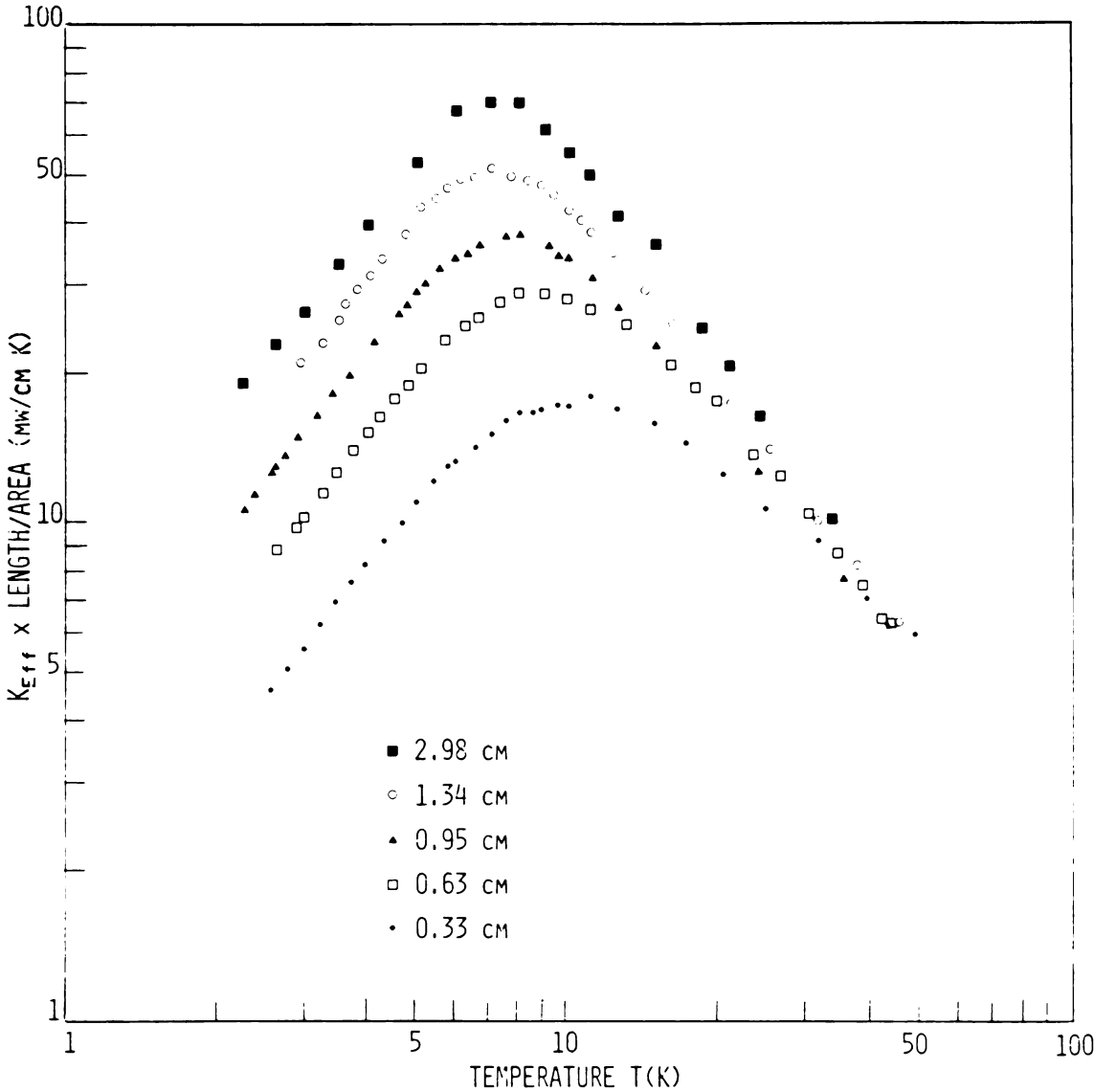

Figure 14. A plot of the effective thermal conductivity versus temperature for samples of different lengths.

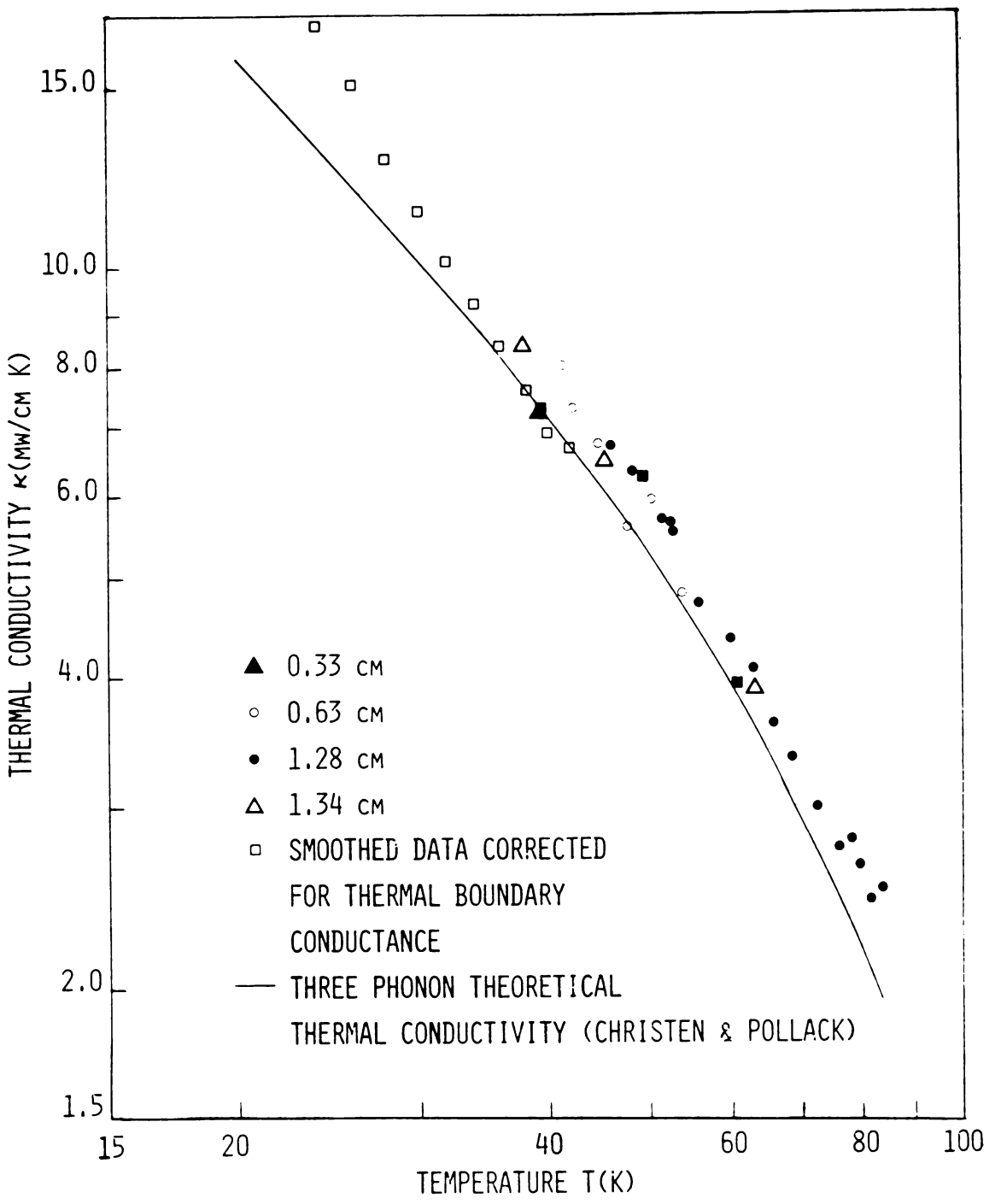

Figure 15. A plot of the high temperature thermal conductivity data and the three-phonon thermal conductivity calculated by Christen and Pollack.

Table 7

Experimental High Temperature Thermal Conductivity Data

T(K)	K_{Eff}(mw/K)	K_{sp}(mw/K)	κ(mw/cm K)
	A. Sample No. 11 Run No. 5		
37.83	5.51	0.05	8.38
45.40	4.28	0.07	6.47
63.45	2.63	0.10	3.89
	B. Sample No. 13 Run No. 1		
39.51	19.26	0.05	7.31
49.53	16.43	0.07	6.23
60.87	10.49	0.09	3.96
	C. Sample No. 15 Run No. 1		
83.08	1.82	0.12	2.51
81.70	1.77	0.12	2.44
79.90	1.90	0.12	2.63
78.27	2.00	0.12	2.78
76.00	1.97	0.11	2.74
72.85	2.14	0.11	3.00
68.72	2.37	0.10	3.35
65.75	2.55	0.10	3.62
62.92	2.86	0.10	4.08
59.65	3.04	0.09	4.35
55.93	3.29	0.09	4.73
52.85	3.83	0.08	5.54
51.34	3.92	0.08	5.68
48.29	4.36	0.07	6.33
45.99	4.61	0.07	6.71
52.50	3.91	0.08	5.66

Table 7 (cont'd)

T(K)	K_{Eff}(mw/K)	K_{sp}(mw/K)	κ(mw/cm K)
	D. Sample No. 17 Run No. 1		
41.38	11.11	0.06	8.03
42.25	10.07	0.06	7.28
44.61	9.34	0.06	6.74
47.61	7.87	0.07	5.60
50.39	8.25	0.07	5.94
53.81	6.72	0.08	4.82
	E. Sample No. 17 Run No. 2		
39.31	2.64	0.05	7.19

Along with these data we also present for comparison the theoretical three phonon $\kappa(T)$ calculation of Christen and Pollack.[24] We should note that between 30 and 80 K the experimental data and the theory are in good agreement. We shall discuss this later.

3. Remarks on the Thermal Conductivity Measurements

The three main features we have just discussed can be understood by recalling some of the unusual properties of solid Ar: (i) the large coefficient of thermal expansion and (ii) the low yield stress. These two properties are clearly manifested by the behavior of $K_{Cont}(T)$ (Figure 13).

Between 4 K and 10 K the relative change in the lattice constant of Ar is negligible (approximately 0.01%)[46] so that for a constant applied force (as is the case here) d and n in Equation (16) should be essentially constant in this temperature range. In the last column of Table 6 we show $K_{Cont}/\kappa = nd$ which does remain essentially constant in this temperature range. Thus $K_{Cont}(T)$ is proportional to κ. This temperature behavior (Figure 13) below 10 K is in quantitative agreement with the results of Moss[47] who measured $\kappa(T)$ of plastically deformed crystals of CaF_2 and found that κ varied somewhat less than T^2.

Above 10 K, n and d are expected to increase with an increase in temperature. This is because the sample as well as the asperities will begin to experience a significant increase in size. In going from 4 K to 20 K the relative increase in the lattice constant is 0.13%, while in

going from 4 K to 40 K it is 0.69%.[46] As the sample increases in length relative to the stationary sample tube ends, the applied force to the sample ends is effectively increased. The increasing force coupled with a diminishing yield stress results in a rapid increase in the contact area above 20 K. Hence, we expect that above 20 K, $K_{Cont}(T)$ and K_{Cont}/κ will both rapidly rise. A quick glance at Figure 13 and at the last column of Table 6 show convincingly that our results support this conclusion.

The first and second effects, (a) and (b), mentioned in the previous section are due mainly to a reduction in the contribution of R (thermal resistance of the sample) because of a reduction in L and also possibly an increase in the thermal conductivity κ for the shorter samples. This latter possibility can be investigated by calculating $\kappa(T)$ separately for the short samples (0.33 cm $\leq$ L $\leq$ 1.34 cm) and long samples (1.97 cm $\leq$ L $\leq$ 2.98 cm). In Figure 16 we have plotted only the meaningful data contained in Table 8.

The plots in Figure 16 indicate that the shorter samples are apparently less damaged (defected) than the larger ones. That is, the thermal conductivity peak of the shorter samples is higher (in fact a factor of 2 higher) and occurs at a lower temperature than for the longer samples. This is consistent with both the experimental observations and the fact that the shorter samples will experience smaller thermal gradients during the cooldown process. This result supports our belief that the thermally induced strains cause

Table 8

Thermal Conductivity Data of Short and Long Samples

	0.33 cm ≤ L ≤ 1.34 cm			1.97 cm ≤ L ≤ 2.98 cm		
T(K)	κ(mw/cm K)	K_{Cont}(mw/K)	Correlation Coefficient	κ(mw/cm K)	K_{Cont}(mw/K)	Correlation Coefficient
2.25	216.6	10.69	0.920	-29.64	3.56	-0.674
2.50	248.7	12.29	0.930	-47.44	4.61	-0.536
2.75	269.0	13.93	0.928	43.54	17.88	0.650
3.00	167.3	15.91	0.726	42.76	24.32	0.734
3.50	173.5	19.61	0.756	49.97	32.81	0.792
4.00	196.2	23.44	0.798	56.24	45.93	0.844
4.50	216.8	27.38	0.803	66.01	54.49	0.864
5.00	260.8	31.23	0.793	76.88	62.94	0.887
5.50	245.3	35.39	0.901	91.29	61.52	0.904
6.00	234.7	39.01	0.944	112.1	52.43	0.909
6.50	215.1	42.16	0.939	124.9	49.02	0.877
7.00	185.8	45.53	0.952	126.1	50.35	0.910
7.50	157.4	48.94	0.962	128.8	48.42	0.917
8.00	136.5	51.89	0.969	123.9	47.80	0.912
8.50	117.9	54.57	0.977	108.7	50.55	0.933
9.00	101.6	57.09	0.983	94.13	54.64	0.946
9.50	88.8	59.38	0.988	83.51	58.23	0.946
10.00	79.1	61.15	0.991	76.13	57.90	0.927

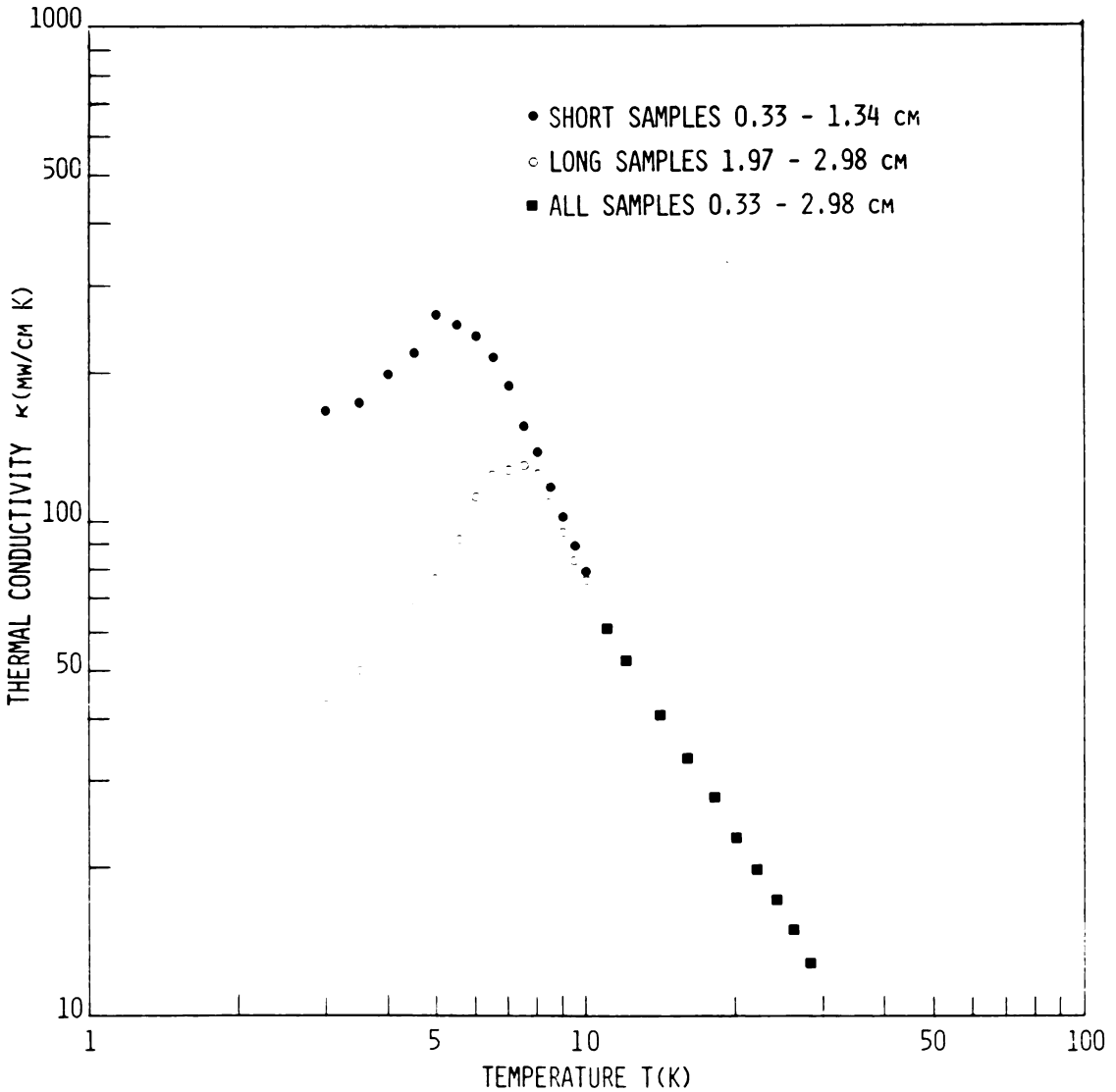

Figure 16. A plot of the calculated thermal conductivity versus temperature for short and long samples.

more damage to the entire sample than pressing on the samples ends.

The third effect (c) we mentioned in the previous section is simply due to the rapid increase in contact area resulting from the combination of the increasing applied force and the reduction of the yield stress of solid Ar. This results in the significant reduction of R_{Cont} relative to R near 38 K for all samples.

4. Thermal Conductivity Errors

In determining κ for Ar from 2.25 K to 65 K we recall that the data were fit to Equation (10) using from 9 to 3 different lengths (See Table 5) for a given isotherm using the method of least squares. For clarity we recall Equation (19)

$$R_{Eff} = mL + R_{Cont} \tag{19}$$

where $R_{Eff} = K_{Eff}^{-1}$, $m = 1/\kappa A$ and $R_{Cont} = 1/K_{Cont}$. Since we were able to measure L directly within ± 0.3%, we will assume that L is known exactly to determine the uncertainty in κ and K_{Cont}. The quantities contributing to the uncertainty are therefore R_{Eff} and A the cross sectional area of the samples.

In this case if the error in R_{Eff} is the same for each length L_i, i.e. $\delta R_{Eff,i} = \delta R_{Eff}$, then the variance of m is given by[48]

$$V(m) = \langle(\delta m)^2\rangle = (\delta R_{Eff})^2/(\sum_i L_i^2 - (\sum_i L_i)^2/N) \tag{20}$$

and the variance of R_{Cont} is given by

$$V(R_{Cont}) = \langle(\delta R_{Cont})^2\rangle$$
$$= (\delta R_{Eff})^2(\Sigma_i L_i^2)/(N\Sigma_i L_i^2 - (\Sigma_i L_i)^2). \quad (21)$$

Ordinarily, if R_{Cont} were exactly reproducible for each run at a given length L_i, then δR_{Eff} would be proportional to $\delta(\Delta T)$. Because of the way in which we smoothed the data, we expect the errors associated with ΔT to average to zero. Hence, the major contribution to the uncertainty in the determination of R_{Eff} is the uncertainty of reproducing the contact resistance δR_{Cont} for each run.

To estimate the maximum uncertainty associated with R_{Cont} we compared the data of sample 14 runs 1 and 2 shown in Figure 17. These two runs we carried out on the same sample for approximately the same length 3.00 cm and 2.98 cm, respectively. We note that for run 1 mechanical contact was lost and then reestablished at 25 K, thus these data were not used in determining κ.

For the expressed purpose of estimating δR_{Cont}, we will assume that κ remained unchanged from run 1 to run 2 and that L and A are known exactly. This is a valid assumption, since the sample was manipulated in essentially the same manner for both runs and annealing between runs is expected to restore the sample to its original unstrained state.[49,50] If we take run 1 to be representative of the maximum value of R_{Cont} and run 2 to be representative of the minimum, then the error in R_{Cont} (or R_{Eff}) is given by,

$$\delta R_{Cont} = \delta R_{Eff} = \pm 1/2\ (R_{Eff,1} - R_{Eff,2}) \quad (22)$$

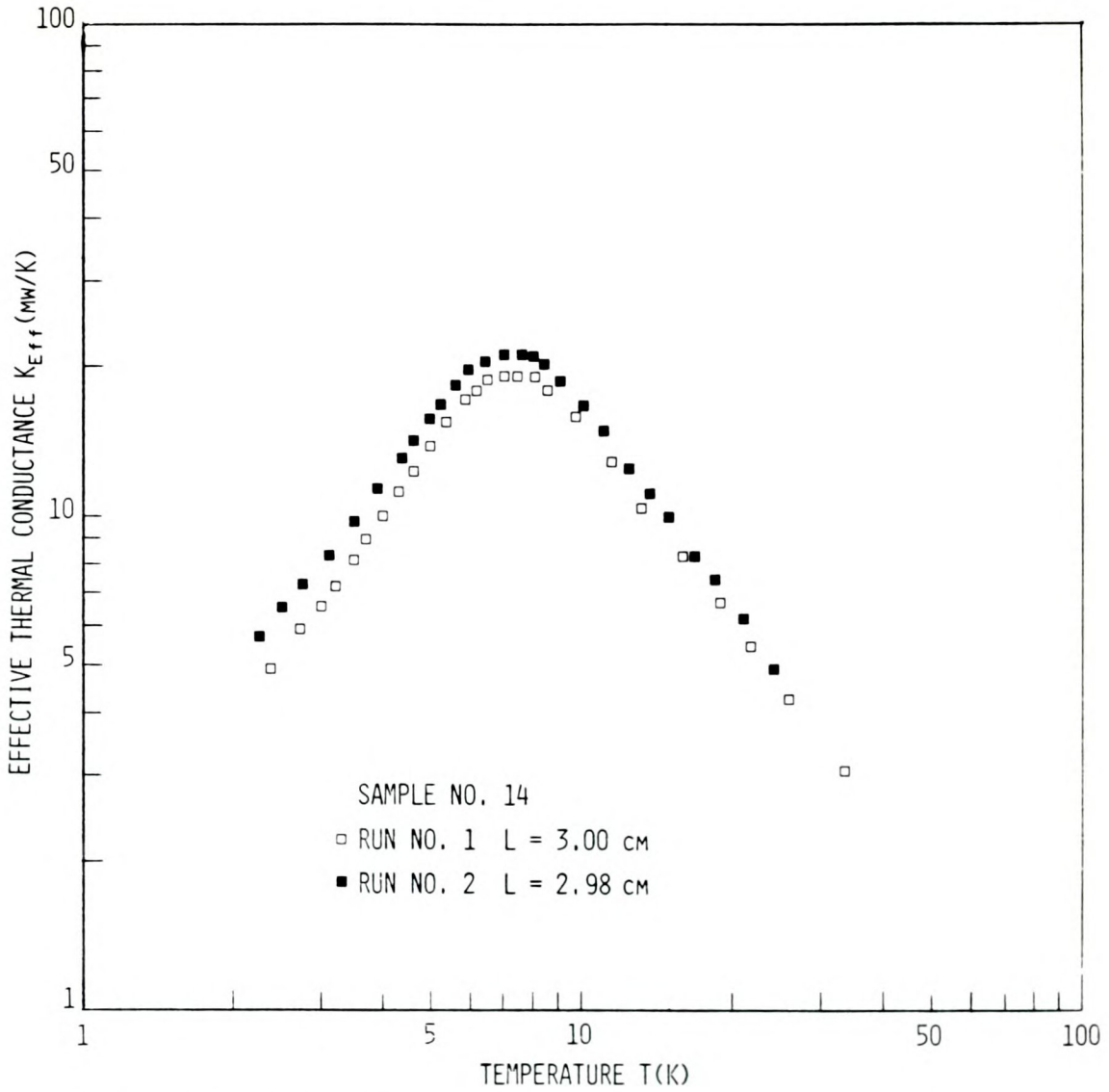

Figure 17. A plot of the effective thermal conductance for two samples of approximately the same length displaying different values of R_{Cont}.

where $R_{Eff,1}$ and $R_{Eff,2}$ are the effective thermal resistances for runs 1 and 2, respectively, at a given temperature. The values of δR_{Eff} determined in this way were found to vary from 0.021 K/mw at 2.25 K to 0.001 K/mw at 40 K.

The fractional error in K_{Cont} is then determined from Equation (19) and the relation

$$\delta K_{Cont}/K_{Cont} = \delta R_{Cont}/R_{Cont} \cdot \qquad (23)$$

The value of $(\delta K_{Cont}/K_{Cont})(100\%)$ was determined to vary from a minimum of 9% at 6 K to a maximum of over 100% above 36 K. This large error near 36 K is just the consequence of R_{Cont} approaching zero as T approaches 38 K. In fact the appearance of the physically unreal, negative values of K_{Cont} in Table 6 in the vicinity of 40 K is just the result of the straight line to which we fit our data, statistically missing zero as the y-intercept.

Since $\kappa = 1/mA$, the fractional error for κ is then given by

$$\delta\kappa/\kappa = \pm (<\delta m^2>/m^2 + (\delta A/A)^2)^{\frac{1}{2}}. \qquad (24)$$

Recalling that $(\delta A/A)(100\%) = 2.0\%$, the values of $(\delta\kappa/\kappa)(100\%)$ were determined to vary from 22% at 2.25 K to $\pm$ 2.0% at 65 K. All of the percentage errors for K_{Cont} and κ are shown in Table 6.

For the raw thermal conductivity data, corrected for the spurious heat conductance (K_{sp}), shown in Table 7 and plotted in Figure 15, we compute the percent error in a straightforward manner. Since for these data

$\kappa = (K_{Eff} - K_{sp})L/A$, the fractional uncertainty in κ is given by

$$\delta\kappa/\kappa = \pm \{(\delta(K_{Eff} - K_{sp})/(K_{Eff} - K_{sp}))^2 + (\delta L/L)^2 + (\delta A/A)^2\}^{\frac{1}{2}} . \quad (25)$$

In a separate experiment with the sample tube and vacuum chamber evacuated we measured K_{sp} directly and found it to vary from 1.11×10^{-1} mw/K at 83 K to 1.10×10^{-2} mw/K at 10 K. The uncertainty in this measurement was less than 0.7% throughout that temperature range. The magnitude of K_{sp} represents a correction of 7% to K_{Eff} at 83 K and a correction of less than 1% at 38 K for a sample of intermediate length, say 1.3 cm. (Since K_{sp} represents less than 1% of the total thermal conductance below 38 K it was unnecessary to correct K_{Eff} data for κ_{sp} at temperatures below 38 K.) Thus the evaluation of Equation (21) gives the result that the percent error for the raw data representing κ is approximately ± 8% for the temperatures between 38 K and 83 K.

IV. DISCUSSION AND CONCLUSION

In the paragraphs that follow we shall briefly discuss how our data compare with the results of previous workers and with the theoretical calculations of Christen[25] and Christen and Pollack.[24] In our concluding remarks we will cite the work of Kimber and Rogers[51], who carried out measurements of κ for constant volume samples of Ne, to aid us in suggesting possibly a better approach to measure the thermal conductivity of Ar.

At high temperatures ($T \geq \Theta$) κ is expected to be proportional to 1/T for a constant volume sample. Clayton and Batchelder who measured κ of isochoric samples of Ar having approximately the same molar volume as ours did indeed find that $\kappa \propto 1/T$ above 20 K. Our data, on the other hand decrease faster than 1/T above 20 K and are in good agreement with the results of Krupskii and Manzhelii[21] (see Figure 11) who found that $1/\kappa = AT + BT^2$ $(A,B > 0)$.

The high temperature, theoretical, κ calculation of Christen and Pollack appears to reconcile the deviation of our data and the data of Krupskii and Manzhelii from the 1/T behavior. In this complicated computer calculation Christen and Pollack[24] used the best known interatomic

potential (Barker and Pompe[52]) to calculate the contribution of the anharmonic components of the crystal potential (three-phonon contribution) to the thermal resistivity. In their calculation, in order to take into account the effects of the lattice expansion, the lattice frequencies were evaluated for the equilibrium density at a given temperature. The results of their calculation are plotted in Figures 15 and 18 along with our data for comparison.

In the temperature range of 30-80 K our data are in reasonable agreement with the three-phonon calculation of Christen and Pollack.[24] However, as the temperature falls below 30 K the theoretical curve (dashed curve in Figure 18) falls significantly below our data. This discrepancy as suggested by Christen and Pollack is probably due to the model used. That is, it was assumed, for this calculation, that the collision frequency for normal processes was much larger than that for Umklapp processes. This has the effect of populating those states which scatter strongly by Umklapp processes, depressing the value of the theoretical κ between 6 K and 30 K.

In the low temperature region for a defective solid dominated by dislocations the expected temperature dependence of κ is T^2. In general below 10 K our data are in qualitative agreement with the constant volume data of Clayton and Batchelder[23] (see Figure 11). However, unlike the T^2 behavior displayed by the data of Clayton and Batchelder, our data show a behavior that is somewhat slower

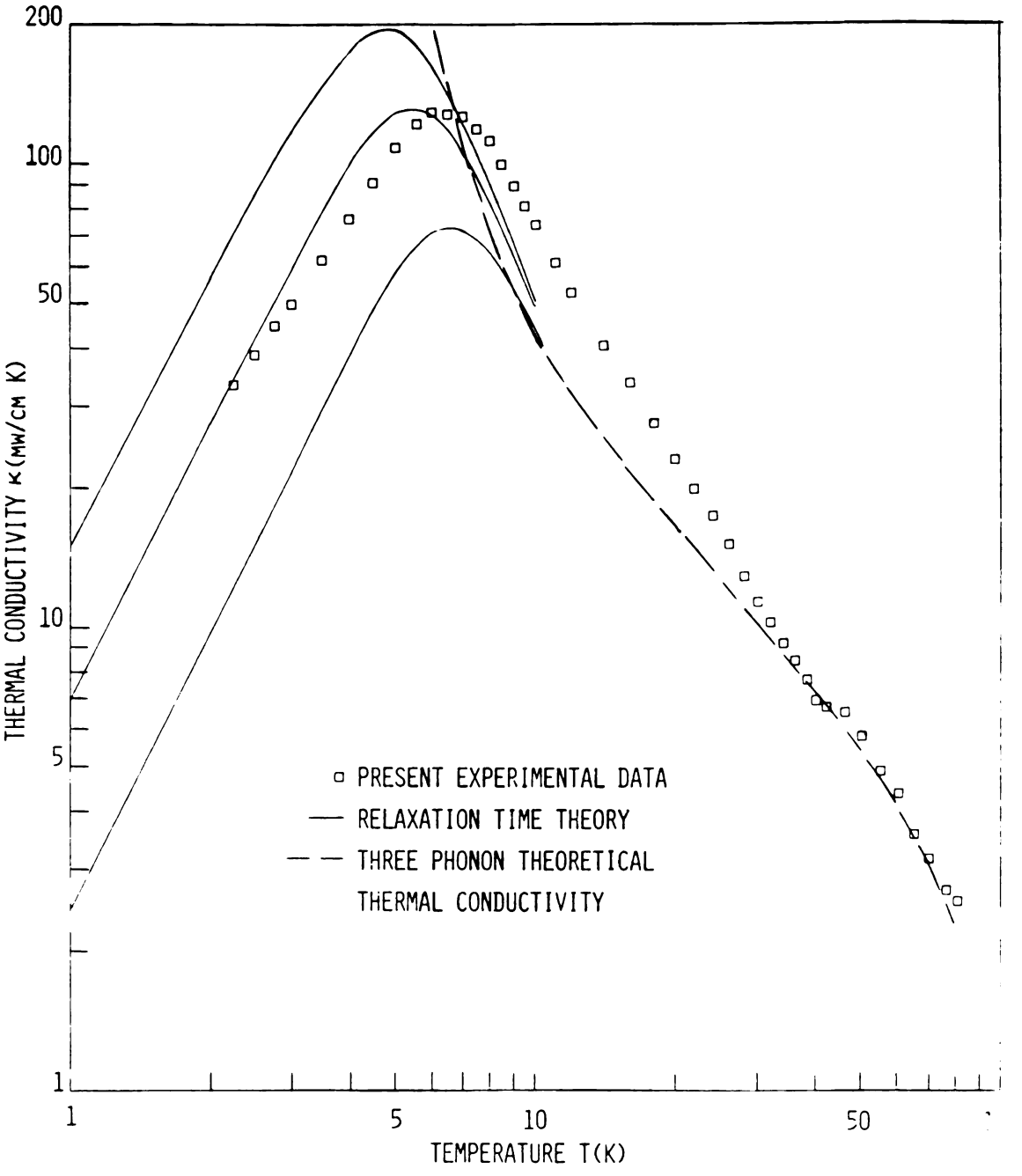

Figure 18. A plot of the low temperature (solid curves) and high temperature (dashed curve) theoretical calculations of Christen and Pollack. Included for comparison are the present data.

than T^2 as the temperature decreases below 5 K. This is the same temperature dependence that was observed by Christen and Pollack. This observed temperature dependence may well be due to the deformed state of the samples we studied. However, since our error in this range is so large this question can only be properly answered after further investigation.

In Figure 18 we have also included the relaxation time theory calculation of Christen, although this theory of low temperature κ is still quite phenomenological. The three solid curves shown in this figure were computed for three different dislocation densities (σ) having values of 2.5×10^9 cm^{-2}, 5.2×10^9 cm^{-2} and 1.5×10^{10} cm^{-2}, respectively, from the uppermost curve to the lowest. These calculations were performed considering only the conventional scattering mechanisms (dislocations, isotopic impurities, sample boundaries and 3 phonon, normal and Umklapp, scattering). The calculations also parametrically take into account the importance that normal processes, relative to the other scattering processes, have in redistributing phonon states among the various scattering mechanisms.

Below 3 K the 1st curve in Figure 18 ($\sigma = 2.5 \times 10^9$ cm^{-2}) is in agreement with the data of Clayton and Batchelder, while below 5 K the 2nd curve ($\sigma = 5.2 \times 10^9$ cm^{-2}) turns out to be in rough agreement (within experimental uncertainty) with our data. Unfortunately, these values are 3 orders of magnitude higher than the values

determined by Peterson, et al.[27] from x-ray analysis of samples of Ar who set a lower limit of $\sigma = 10^6$ cm^{-2}.

To end this part of the discussion we will present the results of previous workers who also carried out equilibrium volume measurements.

In Figure 19 we show a plot of our results along with the data of Bernè, et al.[22] and White and Woods.[19] Between 3 K and 13 K our data do appear to be in reasonable agreement with the data for one of the samples of Bernè, et al. (filled circles). In general, near 20 K, κ is expected to be independent of scattering from defects, however, our data appear to be significantly higher than the results of White and Woods.[19] This difference can probably be attributed to a presence of a thermal contact resistance at the temperature probes, in the data of White and Woods, that was not properly taken into account.

To conclude this discussion we show in Figure 20 the data of Christen and Pollack for their runs 8 and 10 along with the "effective thermal conductivity" ($\kappa_{Eff} = K_{Eff} \times L/A$) of our sample 12 run 1. If there were no thermal contact resistance, from the apparent agreement of the data we would probably, conclude that the thermal conductivity is independent of the cooling rate. This is unlikely since our cooling rates were approximately 70 times those of Christen and Pollack. The more likely explanation is that the thermal contact resistance in the experiments of Christen and Pollack probably changed from run to run.

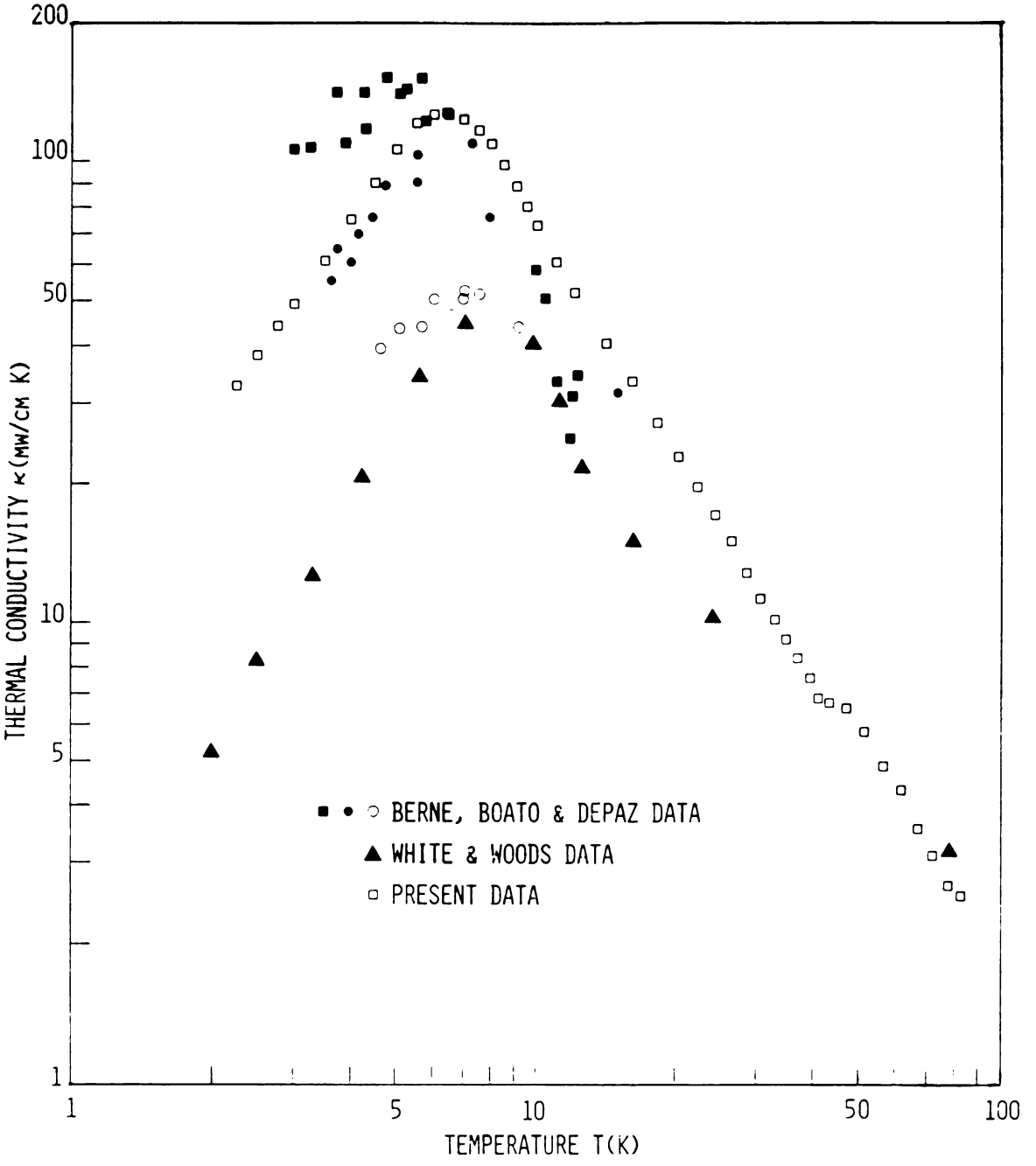

Figure 19. A plot of the thermal conductivity data of several workers for Ar under its own equilibrium vapor pressure.

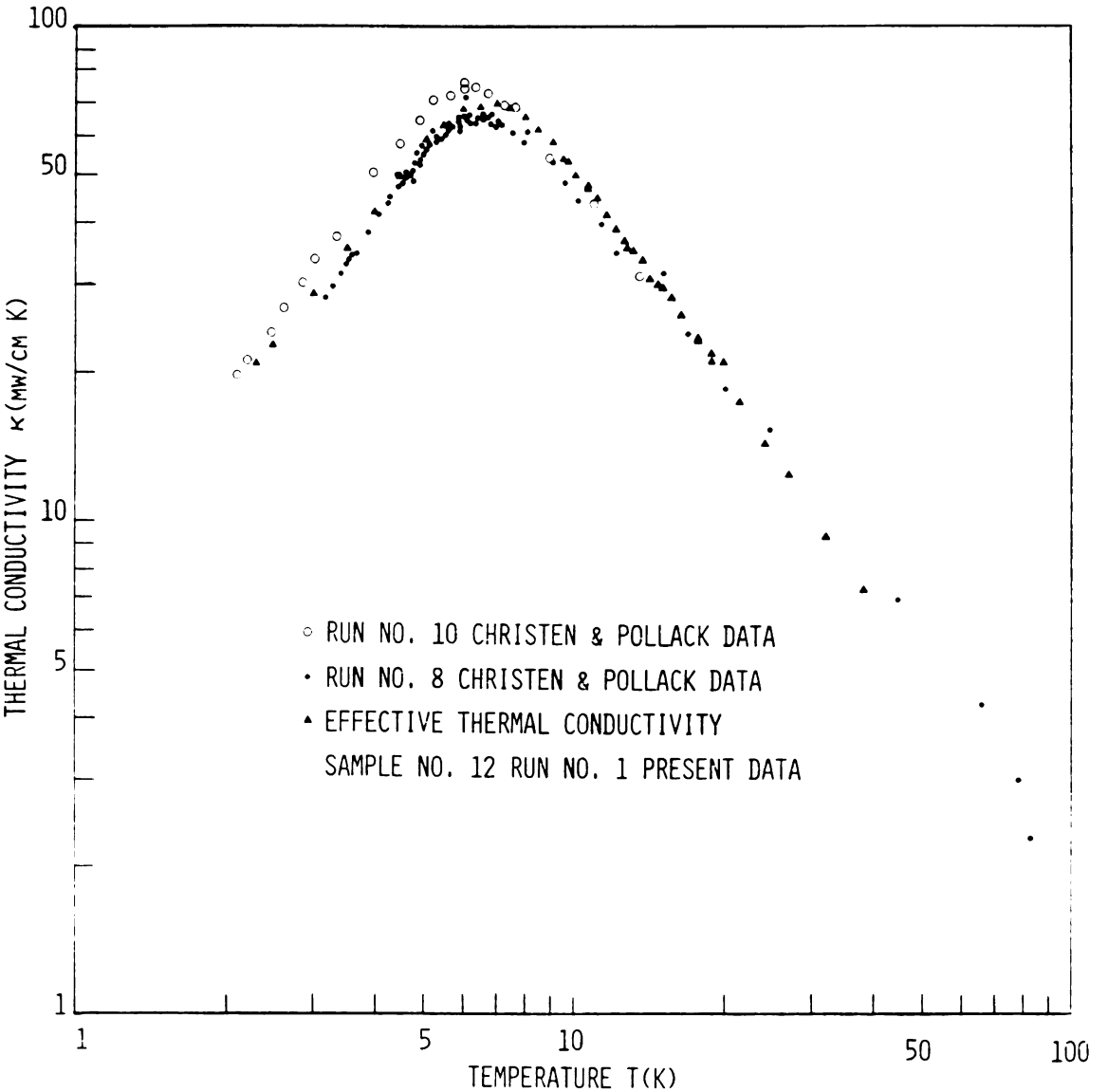

Figure 20. A plot of the thermal conductivity data of Christen and Pollack from runs 8 and 10. Included for comparison is a plot of the "effective thermal conductivity" from the present data, sample 12 run 1.

Figure 21 contains a plot of our data corrected for R_{Cont} including the data of Christen and Pollack for runs 7,8 and 10. The data of run 7 seem to be in agreement with our data and suggest that possibly R_{Cont} for this run was smaller than for the other two.

It is unfortunate that the presence of R_{Cont} masks the true thermal conductivity in measurements of this type, since the quality of the samples studied by Christen and Pollack is probably greater than what the data would imply.

In summary, we have demonstrated that above 38 K the linear heat flow method we have employed yields κ of Ar directly. Unfortunately, at low temperatures (2 to 15 K) R_{Cont} becomes significant and must be reproduced reliably in order to determine κ. In addition, this method yielded only an average value of κ for all of the samples studied. Thus, unless one is willing to work with infinitely large samples, our method will not yield κ directly.

If one is to avoid the complicating effects of a thermal contact resistance a truly potentiometeric method must be used. That is, the probes used to measure ΔT must be in good thermal contact with the sample and must conduct a negligible amount of heat current during the κ measurements.

The experiments carried out on equilibrium volume samples of Ne by Kimber and Rogers[51] employed just such a technique. Kimber and Rogers grew cylindrical samples of Ne in a glass tube (in a manner similar to ours) around

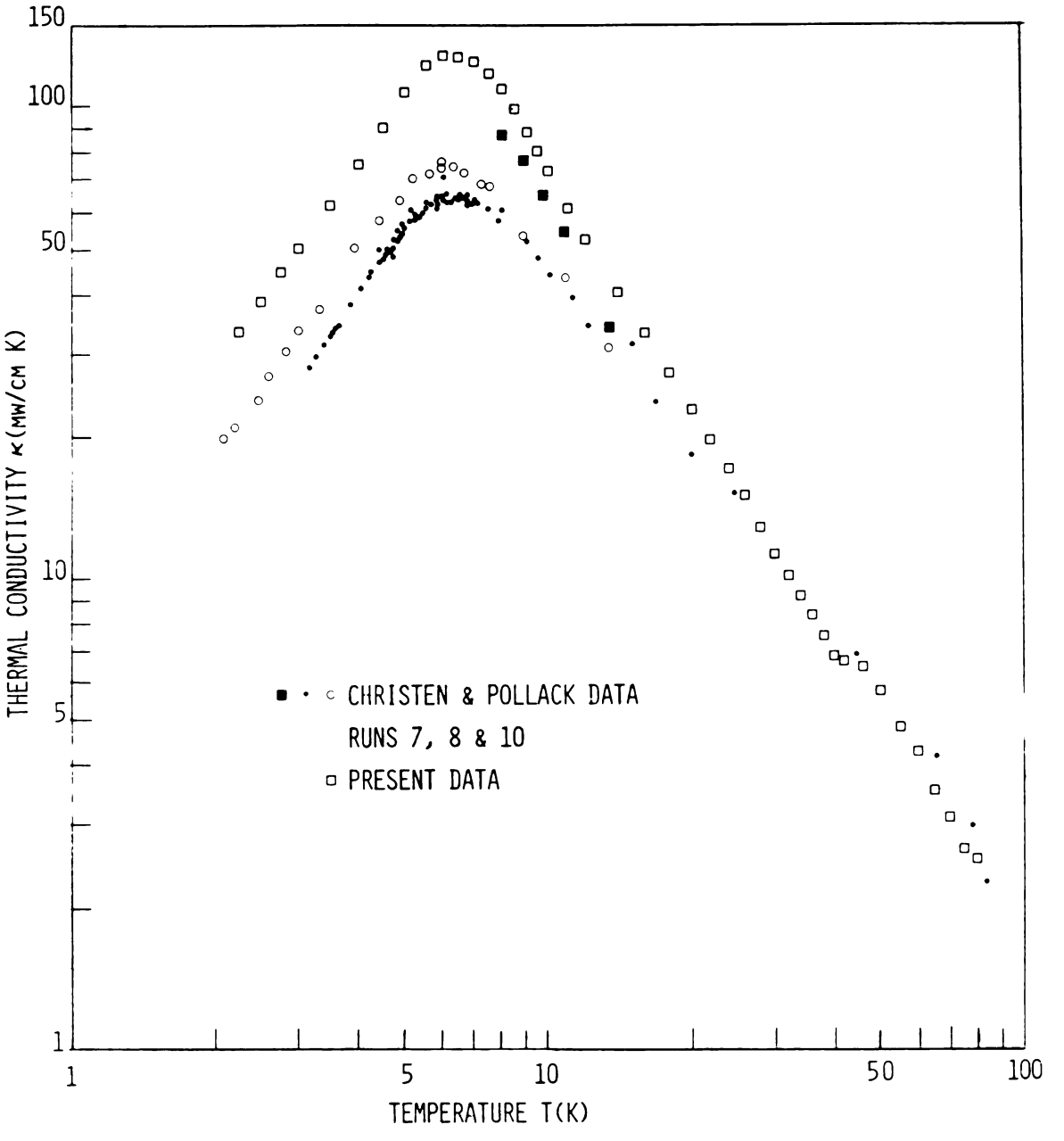

Figure 21. A plot of the thermal conductivity versus temperature of the present data. Included for comparison are the data of Christen and Pollack, runs 7, 8 and 10.

looped platinum wire 0.5 mm in diameter. Before measurements were commenced the samples were first separated from the glass tube and then cooled in a slow and even manner to the temperature range of interest (from 24 K to 4 K in 3 hours). The results for isotopically pure ^{20}Ne samples were in excellent agreement with the results of Clemans[53] who carried out measurements of κ for constant volume samples of ^{20}Ne of the same purity.

In this cleverly designed experiment Clemans had the capability of measuring the κ of the sample in segments and was thus able to test whether the sample was of a uniform quality throughout. The sample chamber used by Clemans consisted of a thick-walled stainless tube with three annular heaters equally spaced one cm apart and a single thermometer located at the bottom was used to measure ΔT. In this way Clemans was able to measure κ for the portion of the sample between the upper heat sink and any one of the three annular heaters during a single run.

The excellent agreement between these two methods, undoubtedly suggests that the successful method used by Kimber and Rogers be employed in future experiments to obtain direct measurements of the thermal conductivity of equilibrium volume samples of Ar.

APPENDICES

APPENDIX A

Table 3

Effective Thermal Conductance at Constant Force

Force Gradually Increased to F_{max} = 30 nt

T(K)	K_{Eff}(mw/K)	T(K)	K_{Eff}(mw/K)
5.01	8.72	5.12	12.17
5.07	8.74	5.12	12.77
5.06	10.57	5.13	13.16
5.05	11.65		

Force = 30 nt

5.13	13.47	6.52	16.05
4.86	12.41	6.80	16.22
4.49	10.64	7.04	16.29
4.14	9.89	7.30	16.45
3.86	8.19	7.57	15.97
3.59	6.87	7.78	16.25
3.94	8.25	8.01	16.37
3.58	7.10	8.27	15.62
3.28	5.62	8.52	15.70
3.27	5.60	8.74	15.73
4.59	9.42	9.00	15.27
4.60	10.27	9.23	15.15
4.61	10.82	9.50	14.94
4.61	10.79	9.76	14.12
4.83	11.66	9.99	14.12
4.99	12.39	10.46	13.46
5.25	13.94	11.00	12.59
5.50	15.05	11.46	12.25
5.79	14.08	12.02	9.63
5.82	14.47	12.96	11.60
6.02	14.53	14.00	10.40
6.26	15.04	15.00	8.59

Table 3 (cont'd)

T(K)	K_{Eff}(mw/K)	T(K)	K_{Eff}(mw/K)
15.01	9.58	9.99	14.57
15.00	9.23	7.96	17.15
17.79	8.01	6.06	17.01
20.04	8.29	6.95	18.68
20.02	6.95	6.95	18.18
20.03	6.53	5.01	14.20
20.03	6.94	5.01	14.34
12.54	11.75	5.01	14.75
12.98	11.01	5.00	14.27
12.01	11.68		
	Applied Force = 15 nt		
5.00	5.88	8.06	10.71
5.00	5.88	8.52	10.36
4.51	4.72	9.08	10.35
4.05	3.66	9.58	10.46
4.05	3.66	10.01	10.00
5.52	6.77	11.04	9.39
6.01	8.09	12.02	8.34
6.48	9.13	12.99	8.14
7.01	9.68	13.98	7.15
7.50	10.36	14.98	6.39

APPENDIX B

Table 4

Effective Thermal Conductance Data

Sample No. 10 Run No. 2

T(K)	K_{Eff}(mw/K)	T(K)	K_{Eff}(mw/K)
5.05	29.03	19.87	14.70
5.05	27.66	21.44	14.23
5.15	28.84	23.32	11.39
5.21	28.00	24.79	11.94
5.50	26.70	26.75	10.44
5.99	29.53	28.61	9.75
6.02	31.83	28.59	8.57
6.26	32.56	28.61	8.80
6.51	32.62	28.61	9.34
6.78	33.00	26.09	10.72
7.00	33.10	24.23	10.41
7.23	33.83	23.14	10.80
7.42	33.74	21.78	13.06
7.44	34.32	20.05	14.52
7.43	33.33	17.88	17.64
7.42	33.38	16.07	20.81
7.41	34.23	14.82	19.84
7.74	32.95	13.78	21.57
8.02	32.77	11.95	23.92
8.20	32.80	11.08	27.32
8.51	32.11	9.98	29.10
9.03	31.73	9.52	30.01
9.52	29.91	9.03	31.51
9.96	28.93	8.52	32.03
11.08	26.89	8.03	32.40
12.00	25.44	7.49	31.57
13.07	23.35	7.03	33.57
14.03	21.11	6.51	32.08
15.30	19.40	6.06	31.02
16.18	18.64	5.73	28.72
17.24	18.33	5.52	28.37

Table 4 (cont'd)

T(K)	K_{Eff}(mw/K)	T(K)	K_{Eff}(mw/K)
5.25	27.58	3.77	18.00
5.01	24.71	3.49	15.95
4.76	24.37	3.27	14.64
4.51	22.09	3.22	15.02
4.52	23.05	3.27	15.15
4.24	21.07	3.27	14.16
4.00	20.49		

Sample No. 11 Run No. 3

4.91	23.84	4.79	21.58
5.00	23.89	4.92	23.24
5.12	24.09	5.01	23.10
5.30	24.56	5.08	24.06
5.45	24.32	4.99	23.94
5.64	24.73	5.13	23.65
4.81	21.21	5.22	24.30
4.67	20.96	5.29	25.41
4.49	19.94	5.41	25.95
4.35	18.72	5.52	25.10
4.21	18.85	5.65	25.34
2.91	11.03	5.81	25.90
2.94	11.97	5.89	26.13
2.98	10.81	5.98	26.25
3.01	11.20	6.09	27.56
3.06	11.66	6.09	27.16
3.16	11.93	6.21	27.04
3.26	12.89	6.43	26.90
3.35	13.42	6.60	27.20
3.47	13.88	6.84	26.27
3.52	13.55	7.03	26.37
3.47	13.81	7.18	27.34
3.53	14.06	7.40	28.72
3.64	14.97	7.56	27.19
3.77	15.61	7.78	26.33
3.87	16.08	8.05	27.09
4.02	16.82	8.24	24.80
4.14	17.77	8.38	25.76
4.27	18.12	8.01	27.06
4.38	18.80	7.38	25.90
4.52	19.40	8.38	23.54
4.64	20.12	8.69	22.98
4.59	20.51	8.86	25.12

Table 4 (cont'd)

T(K)	K_{Eff})mw/K)	T(K)	K_{Eff}(mw/K)
8.84	26.94	11.94	17.91
9.06	25.98	13.08	15.47
9.23	24.93	14.17	15.08
9.56	22.82	15.89	13.10
9.79	21.60	18.36	10.09
9.97	20.57	20.78	8.77
10.55	21.21	24.66	6.54
10.99	19.65		

Sample No. 11 Run No. 5

2.92	14.15	6.47	33.57
2.96	14.27	6.51	34.15
3.00	14.47	6.73	34.38
3.04	14.71	6.99	34.78
3.07	14.95	7.22	34.00
3.16	15.30	7.47	34.20
3.24	15.55	7.77	33.68
3.33	16.41	8.00	33.43
3.40	16.95	8.23	33.26
3.51	17.37	8.55	33.28
3.61	18.56	8.78	32.15
3.73	19.52	8.32	33.11
3.80	19.86	8.65	32.05
3.90	20.50	8.96	32.00
4.03	21.37	9.20	30.85
4.17	22.21	9.37	30.48
4.28	22.99	9.57	29.55
4.42	23.90	9.78	28.76
4.55	24.52	9.96	28.76
4.75	25.51	10.56	27.32
4.95	28.12	11.07	26.00
4.85	27.49	12.29	23.41
5.09	29.01	14.19	19.67
5.26	29.10	16.19	16.91
5.45	30.13	21.15	11.71
5.68	30.08	25.25	9.46
5.64	30.03	31.16	6.82
5.86	29.61	37.83	5.51
5.98	30.26	45.40	4.28
6.12	33.05	63.45	2.63
6.22	32.94		

Table 4 (cont'd)

Sample No. 12 Run No. 1

T(K)	K_{Eff}(mw/K)	T(K)	K_{Eff}(mw/K)
4.67	16.79	4.23	15.00
4.67	16.97	4.35	15.37
4.74	17.22	4.48	15.92
4.89	18.08	4.59	16.63
4.99	18.37	4.69	16.72
5.10	18.83	6.02	21.82
5.20	19.54	6.19	22.03
5.21	19.34	6.47	22.14
5.33	19.83	6.62	22.31
5.47	20.24	6.87	22.14
5.58	20.96	7.00	22.31
5.66	21.18	7.27	22.13
5.76	20.96	7.46	21.93
5.85	21.38	7.66	21.88
5.94	21.73	7.85	21.75
6.02	21.77	8.01	21.24
6.08	21.96	8.25	20.42
6.17	22.09	8.48	19.95
6.27	22.44	8.71	19.42
6.37	22.20	8.90	18.86
2.30	6.70	9.04	18.62
2.35	6.74	9.24	18.06
2.40	6.99	9.49	17.35
2.47	7.27	9.70	17.03
2.54	7.60	10.04	16.07
2.61	7.87	10.63	14.93
2.68	8.19	11.09	14.17
2.77	8.52	11.59	13.29
2.85	8.80	12.07	12.47
2.93	9.10	12.69	11.52
2.99	9.25	13.11	11.15
3.08	9.71	14.25	9.91
3.13	9.88	15.10	9.14
3.21	10.05	10.60	15.30
3.29	10.34	11.04	14.28
3.38	11.03	12.57	11.91
3.50	11.43	13.71	10.67
3.63	12.05	14.73	9.63
3.75	12.52	15.65	8.75
3.86	13.07	16.41	8.32
3.97	13.58	17.65	7.53
4.10	14.21	18.71	6.63

Table 4 (cont'd)

T(K)	K_{Eff}(mw/K)	T(K)	K_{Eff}(mw/K)
17.70	7.38	24.19	4.61
18.79	6.99	26.93	4.00
19.95	6.73	32.00	3.02
21.52	5.54	37.87	2.33

Sample No. 13 Run No. 1

4.59	27.01	7.55	44.29
4.69	27.51	6.02	36.55
4.87	29.06	8.03	45.66
5.02	30.11	8.51	45.61
5.18	31.22	8.93	46.64
4.32	24.98	9.51	47.06
3.97	22.41	10.01	46.90
3.70	20.61	11.07	49.09
3.48	18.98	12.51	46.23
3.23	17.10	14.94	43.47
2.98	15.23	17.16	39.60
2.77	13.95	20.31	37.13
2.57	12.63	24.85	29.17
5.40	33.17	31.36	25.23
5.76	35.55	39.51	19.26
5.98	36.06	49.53	16.43
6.55	38.81	60.87	10.49
7.06	41.32		

Sample No. 13 Run No. 3

4.42	23.92	5.00	27.65
4.61	24.96	5.20	28.65
4.79	26.07	5.52	29.21
4.14	22.00	5.82	32.50
3.90	20.38	5.56	30.95
3.68	18.89	5.98	32.26
3.41	17.28	6.27	33.07
3.18	15.56	6.52	33.74
2.90	13.61	6.73	34.26
2.75	13.00	7.03	37.26
2.28	10.14	7.49	35.55
2.39	10.86	7.96	36.82
2.49	11.45	8.49	35.46
2.62	12.33	9.05	34.28

Table 4 (cont'd)

T(K)	K_{Eff}(mw/K)	T(K)	K_{Eff}(mw/K)
9.51	32.75	15.01	21.56
10.01	32.19	23.84	11.85
11.08	29.69	28.16	10.22
12.56	26.48	35.20	7.32

Sample No. 14 Run No. 1

4.61	12.35	6.71	18.85
4.76	13.04	6.87	18.84
4.96	13.88	7.02	19.05
5.20	14.88	7.20	19.13
4.29	11.17	7.41	19.13
4.42	11.67	7.65	19.22
4.54	12.25	7.87	19.15
3.99	10.01	8.03	19.05
4.08	10.40	8.28	18.55
4.19	10.75	8.56	17.94
2.39	4.92	8.80	17.50
2.49	5.22	9.03	17.00
2.59	5.54	9.28	16.53
2.73	5.94	9.50	16.22
2.88	6.34	9.72	15.61
2.99	6.57	9.74	15.79
3.11	6.93	9.99	15.42
3.22	7.18	10.37	14.58
3.34	7.70	10.53	14.25
3.48	8.16	11.09	13.75
3.70	8.95	11.85	12.39
3.80	9.31	11.46	12.82
3.94	9.87	13.21	10.43
5.16	14.52	12.39	11.51
5.36	15.49	14.20	9.81
5.48	15.92	15.23	9.13
5.66	16.75	15.91	8.31
5.84	17.12	18.80	6.75
6.03	17.74	21.57	5.44
6.18	17.85	25.90	4.30
6.36	18.32	33.26	3.06
6.57	18.88		

Table 4 (cont'd)

Sample No. 14 Run No. 2

T(K)	K_{Eff}(mw/K)	T(K)	K_{Eff}(mw/K)
4.60	14.34	5.92	19.79
4.60	14.35	6.05	20.05
4.70	14.79	6.23	20.41
4.85	15.41	6.40	20.61
4.96	15.73	6.61	20.89
5.07	16.46	6.77	21.02
5.16	16.83	7.02	21.25
5.28	16.44	7.23	21.20
2.28	5.76	7.54	21.43
2.37	6.08	7.75	21.43
2.50	6.55	8.03	21.01
2.62	6.90	8.30	20.27
2.75	7.30	8.74	19.36
2.90	7.73	8.97	18.67
3.01	8.01	9.35	17.81
3.09	8.24	9.67	17.32
3.22	8.78	9.90	16.85
3.29	9.03	10.30	15.86
3.38	9.34	6.03	20.01
3.50	9.81	6.50	20.79
3.55	9.98	7.02	21.27
3.63	10.29	7.45	21.23
3.76	10.69	7.97	21.16
3.90	11.38	8.99	18.64
4.03	11.82	10.08	16.58
4.14	12.39	10.58	15.69
4.23	12.63	11.01	14.90
2.36	13.26	11.95	13.24
4.55	14.09	12.56	12.42
5.40	17.81	13.62	11.14
5.52	18.27	15.01	9.90
5.64	18.95	16.69	8.39
5.73	19.18	18.53	7.46
5.83	19.79	20.92	6.36
5.93	19.83	23.88	4.98
6.06	20.10		

Table 4 (cont'd)

Sample No. 15 Run No. 1

(T)	K_{Eff})mw/K)	T(K)	K_{Eff}(mw/K)
83.08	1.82	62.92	2.86
81.70	1.77	59.65	3.04
79.90	1.90	55.93	3.29
78.27	2.00	52.85	3.83
76.00	1.97	51.34	3.92
72.85	2.14	48.29	4.36
68.72	2.37	45.99	4.61
65.75	2.55	52.50	3.91

Sample No. 16 Run No. 1

4.66	26.86	9.00	42.23
4.88	27.60	9.46	41.47
5.12	29.74	9.98	40.77
5.44	32.91	10.48	40.66
2.59	12.50	11.04	39.18
2.65	12.89	11.97	37.48
2.87	14.20	13.16	36.20
3.00	14.93	13.99	33.65
3.27	16.83	14.94	32.80
3.50	18.43	16.14	30.16
3.77	20.39	18.02	27.46
4.02	22.25	20.08	25.44
4.26	23.91	23.40	19.86
4.42	24.98	25.11	17.77
4.54	26.02	26.87	18.09
4.75	27.45	28.20	17.30
5.00	29.03	30.21	15.32
5.48	32.41	32.18	13.94
5.69	33.94	34.42	12.56
5.99	35.43	36.23	11.84
6.28	36.44	38.14	10.97
6.66	37.89	41.38	11.11
6.99	39.31	42.25	10.07
7.39	40.54	44.61	9.34
7.81	42.54	47.61	7.87
8.01	42.00	50.23	7.37
8.50	41.96	53.81	6.72

Table 4 (cont'd)

Sample No. 16 Run No. 2

T(K)	K_{Eff}(mw/K)	T(K)	K_{Eff}(mw/K)
4.69	16.39	6.67	22.36
4.82	17.82	6.82	22.31
4.99	17.98	7.01	22.21
5.23	19.07	7.22	22.39
5.40	19.86	7.41	22.30
2.47	6.09	7.72	22.26
2.62	6.76	7.94	22.12
2.79	7.48	8.21	21.56
3.00	8.24	8.46	20.87
3.25	9.17	8.71	20.14
3.46	10.42	8.97	19.41
3.76	11.81	9.14	19.23
4.01	13.18	9.39	18.78
4.23	14.20	9.70	18.29
4.50	15.48	10.00	17.73
4.78	16.77	10.35	17.53
4.32	14.51	10.78	16.39
4.62	16.15	11.06	16.02
4.82	17.09	12.02	14.12
5.12	18.47	12.82	12.92
5.29	19.06	14.16	11.69
5.51	20.09	15.11	10.60
5.66	20.70	16.09	9.71
5.75	21.28	18.42	8.69
6.00	21.66	20.66	7.18
6.15	21.55	22.63	6.16
5.99	21.15	24.27	5.36
5.83	21.04	27.15	4.82
5.65	20.43	29.65	4.09
6.00	21.13	34.43	3.23
6.32	21.69	39.31	2.64
6.47	21.88		

APPENDIX C

Defect Scattering - Classical Analogs

1. Rayleigh Scattering from a Spherical Object - Dimensional Analysis

The Rayleigh scattering law for a spherical obstruction can be verified by energy conservation and dimensional analysis considerations.[15] Consider a plane wave of unit amplitude $\psi_i = \exp(iqz)$ incident upon a spherical object of volume V such that $\lambda >> V^{1/3}$. The amplitude of the scattered wave ψ_s is necessarily proportional to 1/r since the scattering intensity is proportional to $|\psi_s|^2$ and $|\psi_s|^2 \propto 1/r^2$. This is because $\int_\Omega |\psi_s|^2 r^2 d\Omega$ must be equal to a constant. Now the only other quantities that ψ_s can depend on are υ (velocity of sound), λ (wavelength) given by $2\pi q^{-1}$ and V (volume). Since υ is the only quantity that involves time as one of its dimensions, it is discarded. Hence, the simplest product that we can form from λ, r and V such that ψ_s remains dimensionless is $V/\lambda^2 r = L^3/L^2 L = 1$. Thus, $\psi_s \propto V/\lambda^2 r$ and the scattering cross section is proportional to V^2/λ^4. That is, σ is proportional to q^4.

2. Scattering from a Cylindrical Object - Dimensional Analysis

The Rayleigh scattering law for an infinite cylindrical obstruction can be verified as in the preceding case.[15] In this instance since we have cylindrical symmetry, the problem can be reduced to 2 dimensions. Scattering intensity considerations yield that the amplitude of $\psi_s \propto 1/\rho^{\frac{1}{2}}$, since $\int_\theta |\psi_s|^2 \rho d\theta$ must be a constant. The other quantities on which ψ_s can depend are λ and $A = \pi a^2$ the cross sectional area of the cylinder. Thus the simplest product we can form is $A/\lambda^{3/2}\rho^{\frac{1}{2}}$, i.e., $\psi_s \propto A/\lambda^{3/2}\rho^{\frac{1}{2}} = L^2/L^{3/2}L^{\frac{1}{2}} = 1$. Therefore, the core scattering cross section per unit length of dislocation is $\sigma_{core} \propto |\psi_s|^2 \sim A^2/\lambda^3 = a(a/\lambda)^3$.

3. Scattering from the Strain Field Surrounding the Cylindrical Core - Geometrical "Optics" Limit

For a phonon that is deviated from its original direction by an angle $\phi \sim \gamma b/p$ on passing through the strain field, the change in momentum along the original direction is proportional to $(1-\cos\phi)$.[32] Since the change in heat current will be reduced by an amount which is proportional to $(1-\cos\phi)$, the scattering cross section per unit length of dislocation is thus proportional to

$$\int_0^{\phi_m} (1-\cos\phi)\, d\phi \simeq \int_\infty^{p_0} (\gamma b/p)^2 dp \simeq \gamma^2 b^2/p_0$$

where p_0 is the least value of p ($p_0 \sim \lambda$). Thus σ_{strain} is proportional to $\gamma^2 b^2/\lambda$.

APPENDIX D

Error Associated with the Magnitude of ΔT

In our measurements the expression we use to evaluate the effective thermal conductance is given by

$$K_{Eff}\ (\bar{T}) = \dot{Q}/\Delta T \qquad (D1)$$

where $\bar{T} = T_0 + \Delta T/2$ is the average temperature. For small ΔT Equation (D1) is a good approximation of the following equation

$$K_{Eff} = \dot{Q}/\Delta T = \left(\int_{T_0}^{T_0+\Delta T} K(T)\,dT\right)/\Delta T \qquad (D2)$$

where $K(T)$ is the true effective thermal conductance.[14,25]

At low temperatures $K(T) \simeq AT^2$. On substituting this expression into Equation (D2) and evaluating the integral we obtain for the effective thermal conductance

$$K_{Eff} = ((T_0 + \Delta T)^3 - T_0^3)A/3\Delta T\ . \qquad (D3)$$

The true effective thermal conductance at $\bar{T}$ is given by

$$K(\bar{T}) = A(T_0 + \Delta T/2)^2\ . \qquad (D4)$$

The relative difference $(K(\bar{T}) - K_{Eff})/K(\bar{T})$ to lowest order in $\Delta T/T_0$ is given by

$$\Delta K/K \simeq (\Delta T/T_0)^2/12\ . \qquad (D5)$$

Hence, if we want Equation (D1) to stay within 1% of the

true effective thermal conductance, then the largest ΔT that we should not exceed at the lowest temperature (2 K) is given by

$$\Delta T \leq 2(0.12)^{\frac{1}{2}} = 0.7 \text{ K} . \qquad \text{(D6)}$$

Similarly at the highest temperatures, where $K \simeq BT^{-1}$ after performing the appropriate expansions, the error will also be given to lowest order in $\Delta T/T_0$ by Equation (D5). Hence, if at 80 K we wish to stay within a 1% error, then the largest ΔT that we should not exceed is given by

$$T \leq 80(0.12)^{\frac{1}{2}} = 28 \text{ K}.$$

LIST OF REFERENCES

LIST OF REFERENCES

1. H. Cavendish, Phil. Trans. R. Soc., 75, 372 (1785).

2. G. A. Cook in Argon, Helium, and the Rare Gases I, G. A. Cook ed., (Interscience Publishers, New York, 1961).

3. G. K. Horton in Rare Gas Solids 1, J. A. Venables and B. L. Smith eds., (Academic Press, London, 1977).

4. G. L. Pollack, Biophysical J. 19, 49 (1977).

5. J. Unsworth and F.C. Gillespie in Diffusion Processes 2, J. N. Sherwood, et al. eds., (Gordon & Breach, Science Publishers, Inc., New York, 1971).

6. D. A. Nelson and A. L. Ruoff, Phys. Rev. Lett. 42, 383 (1979).

7. D. N. Batchelder in Rare Gas Solids 2, J. A. Venables and B. L. Smith eds., (Academic Press, London, 1977).

8. G. L. Pollack, Rev. Mod. Phys. 41, 48 (1969).

9. R. E. Peierls, Quantum Theory of Solids (Oxford University Press, New York, 1964).

10. P. Carruthers, Rev. Mod. Phys. 33, 92 (1961).

11. C. Kittel, Introduction to Solid State Physics (John Wiley and Sons, Inc., New York, 1971).

12. R. E. Peierls, Ann. Phys. Leipzig 3, 1055, 1101 (1929).

13. P. G. Klemens in Thermal Conductivity 1, R. P. Tye ed., (Academic Press, New York, 1969).

14. R. Berman, Thermal Conduction in Solids (Oxford University Press, Oxford, 1976).

15. Lord Rayleigh, Theory of Sound 2 (Dover Publications, New York, 1945).

16. F. R. N. Nabarro, Proc. Roy. Soc. A209, 278 (1951).

17. J. M. Ziman, Nuovo Cimento 7, 353 (1958).

18. B. L. Smith, Contemp. Phys. 11, 125 (1970).

19. G. K. White and S. B. Woods, Phil. Mag. 3, 785 (1958).

20. I. N. Krupskii, V. G. Manzhelii, and L. A. Koloskova, Phys. Stat. Sol. 27, 263 (1968).

21 I. N. Krupskii and V. G. Manzhelii, Phys. Stat. Sol. 24, K53 (1967) and Soviet Phys. JETP, 28, 1097 (1969).

22. A. Bernè, G. Boato and M. DePaz, Nuovo Cimento 46, 182 (1969).

23. F. Clayton and D. N. Batchelder, J. Phys. C6, 1213 (1973).

24. D. K. Christen and G. L. Pollack, Phys. Rev. B12, 338 (1975).

25. D. K. Christen, Thermal Conductivity of Solid Argon, Ph.D. Thesis, Michigan State University (1974).

26. J. A. Venables and B. L. Smith in Rare Gas Solids 2, J. A. Venables and B. L. Smith eds., (Academic Press, London, (1977).

27. O. G. Peterson, D. N. Batchelder and R. O. Simmons, J. Appl. Phys. 36, 2682 (1965).

28. G. K. White and S. B. Woods, Canad. J. Phys. 33, 58 (1955) and Nature, London 177, 851 (1956).

29. R. K. Crawford and W. B. Daniels, J. Chem. Phys. 50, 3171-83 (1969).

30. W. B. Daniels, et al., Phys. Rev. Lett. 18, 548-50 (1967).

31. J. A. Leake, et al., Phys. Rev. 181, 1251-60 (1969).

32. J. M. Ziman, Electrons and Phonons (Clarendon Press, Oxford, 1960).

33. G. K. White, Experimental Techniques in Low-Temperature Physics (Clarendon Press, Oxford, England, 1968).

34. A. C. Rose-Innes, Low Temperature Techniques, (English University Press, Ltd., London, 1964).

35. V. I. Grushko, D. N. Bol'shutkin, G. N. Scherbakov and N. F. Shevchenko, Soviet Phys.-Crystallography 15, 536 (1970).

36. M. Gsänger, H. Egger, G. Fritsch and E. Lüscher, Z. Angew. Phys. 26, 334 (1969).

37. G. L. Pollack and E. N. Farabaugh, J. Appl. Phys. 36, 513 (1965).

38. I. Lefkowitz, K. Kramer, M. A. Shields and G. L. Pollack, J. Appl. Phys. 38, 4867 (1967).

39. G. L. Pollack and H. P. Broida, J. Chem. Phys. 38, 968 (1963).

40. C. R. Tilford and C. A. Swenson, Phys. Rev. B5, 719 (1772).

41 R. Berman, J. Appl. Phys., 27, 318 (1956).

42. A. V. Leonteva, Yu. S. Stroilov, E. E. Lakin and D. N. Bol'shutkin, Phys. Stat. Sol. 42, 543 (1970).

43. R. Berman and C. F. Mate, Nature, Lond., 182, 1661 (1958).

44. C. F. Mate in "Heat Flow below 100 K", p. 101, Annexe. 1965-2 Suppl. Bull. Inst. Refrig. (1965).

45. D. Tabor, The Hardness of Metals (Oxford University Press, 1951).

46. O. G. Peterson, D. N. Batchelder and R. O. Simmons, Phys. Rev. 150, 703 (1966).

47. M. Moss, J. Appl. Phys. 36, 3308 (1965).

48. S. L. Meyer, Data Analysis for Scientist and Engineers, (John Wiley and Sons, Inc., New York, 1975).

49. W. R. G. Kemp, P. G. Klemens and R. J. Tanish, Phil. Mag. 4, 845 (1959).

50. J. N. Lomer and H. M. Rosenberg, Phil. Mag. 4, 467 (1959).

51. R. M. Kimber and S. J. Rogers, J. Phys. C6, 2279 (1973).

52. J. A. Barker and A. Pompe, Australian J. Chem. 21, 1683 (1968).

53. J. E. Clemans, Phys. Rev. B 15, 1072 (1975).

54. G. Boato, Cryogenics 4, 65 (1964).